European Cells and Materials Vol.49 2025 (pages 35–54) DOI: 10.22203/eCM.v049a05 ISSN 1473-2262

Original Article

ELECTROSPUN BIOACTIVE POLY(ε-CAPROLACTONE) NANOFIBROUS SCAFFOLDS INCORPORATED WITH NATURAL DECELLULARIZED BONE EXTRACELLULAR MATRIX FOR BONE REGENERATION

M. Zhang[1,2,§], Q. Zhou[3,§], Q.S. Dong[4], J. Zhang[5], X. Zhou[5], H. Huang[5], J.C. Bao[5], H.J. Shan[5], F.R. Sun[5] and L.L. Li[1,*]

[1]Department of Orthopaedic Surgery, The Second Hospital of Nanjing, 210003 Nanjing, Jiangsu, China
[2]Department of Orthopaedics, Zhongda Hospital, School of Medicine, Southeast University, 210009 Nanjing, Jiangsu, China
[3]Department of Orthopaedic Surgery, The Affiliated Huai'an Hospital of Xuzhou Medical University, The Second People's Hospital of Huai'an, 223002 Huai'an, Jiangsu, China
[4]School of Materials Science and Engineering, Jiangsu Key Laboratory of Advanced Structural Materials and Application Technology, Nanjing Institute of Technology, 211167 Nanjing, Jiangsu, China
[5]Department of Orthopaedic Surgery, The Affiliated Jiangning Hospital of Nanjing Medical University, 211100 Nanjing, Jiangsu, China
[§]These authors contributed equally.

Abstract

Background: Cell-free bone tissue scaffolds show significant potential for bone repair applications. This study aimed to enhance the bone regeneration performance of synthetic poly(ε-caprolactone) (PCL)-based nanofibrous scaffolds by incorporating natural decellularized bone extracellular matrix (dB-ECM) into the scaffold. **Methods:** The PCL/dB-ECM nanofibrous scaffolds were fabricated by electrospinning. A series of *in vitro* and *in vivo* experiments were conducted to verify the biocompatibility of the PCL/dB-ECM nanofibrous scaffolds, as well as their ability to promote osteogenic differentiation of rabbit bone mesenchymal stem cells (rBMSCs) and to repair bone defects. **Results:** The incorporation of dB-ECM significantly enhanced the bioactivity of the PCL-based scaffold, yielding superior rBMSCs attachment and proliferation, cytoskeleton extension, and osteogenic differentiation. Furthermore, *in vivo* assays revealed that the PCL/dB-ECM (2:1) scaffold facilitated new bone formation, with improved trabecular structures and better integration with the surrounding tissues. **Conclusions:** The PCL/dB-ECM (2:1) nanofibrous scaffold presents a promising strategy for bone defect repair, offering enhanced bioactivity and effective integration with host tissues.

Keywords: Bone regeneration, nanofibrous scaffold, decellularized extracellular matrix, poly(ε-caprolactone), electrospinning.

***Address for correspondence**: L.L. Li, Department of Orthopaedic Surgery, The Second Hospital of Nanjing, 210003 Nanjing, Jiangsu, China. Email: liangliangliinj@163.com.

Copyright policy: © 2025 The Author(s). Published by Forum Multimedia Publishing, LLC. This article is distributed in accordance with Creative Commons Attribution Licence (http://creativecommons.org/licenses/by/4.0/).

Introduction

Critical-sized bone defects, typically resulting from trauma, bone tumors, or extensive surgical resections, continue to pose a substantial challenge in orthopedic surgery [1,2]. Bone grafts rank as the second most frequently transplanted tissue in the United States [3]. Although autogenous bone grafts are considered the gold standard for treating critical-size bone defects, they are not without drawbacks. These include limited availability of donor tissue, donor site morbidity, and poor availability [4–6]. Consequently, there is an urgent need to develop bioactive substitutes for bone-defect repair.

Bone tissue engineering (BTE) aims to create artificial substitutes for critical-sized bone defects. Cell-free BTE scaffolds offer new avenues in biomaterial design for bone repair. The structural design and choice of biomaterials are crucial for enhancing cellular responses and promoting tissue generation in cell-free BTE scaffolds. Recently, several advanced technologies have been developed to fabricate scaffolds with precise structural properties. These technologies include three dimension (3D) printing, electrospinning, freeze-drying, and selective laser sintering [7–9]. Among these, electrospinning stands out as a versatile method for producing nanofibrous scaffolds with a high surface-area-to-volume ratio and optimal fiber spac-

ing, providing an ideal platform for cell adhesion, proliferation, and differentiation [10,11]. Importantly, electrospun nanofibrous scaffolds closely mimic the native structure of the extracellular matrix (ECM), which is essential for cell survival, migration, and proliferation [12]. Therefore, electrospinning is widely used in drug delivery systems, wound dressings, and scaffold fabrication [13,14].

Both natural and synthetic polymers are used in BTE scaffolds [15]. Natural polymers, such as collagen, gelatin, silk, hyaluronic acid, alginate, and decellularized tissues, are favored for their hydrophilicity, biocompatibility, and osteoinductive properties. However, their antigenicity, poor mechanical strength, and rapid degradation limit their effectiveness in BTE applications [16]. In contrast, synthetic polymers like poly(ε-caprolactone) (PCL), poly(lactic acid) (PLA), poly(lactic-co-glycolic acid) (PLGA) and their copolymers offer better biocompatibility, controlled degradation, and support for neovascularization and bone formation [17,18]. Among these, PCL is particularly notable for its mechanical strength, biocompatibility, and Food and Drug Administration (FDA) approval for use in biomedical devices [17,19]. Additionally, the rough surface of PCL promotes initial cell anchoring [20]. Despite these advantages, pure PCL suffers from low hydrophilicity and limited biochemical activity, which can hinder scaffold-cell interactions and ECM deposition [21,22]. To address these limitations, strategies such as PCL-based blend scaffold fabrication and surface modification have been used to improve the hydrophilicity and bioactivity of PCL [23,24].

While electrospun PCL nanofibrous scaffolds mimic ECM-like structures, they lack the bioactivity inherent to natural ECM. Decellularized bone extracellular matrix (dB-ECM), derived from bone tissue and composed of inorganic hydroxyapatite mineral and organic matrix components [25], has shown significant potential in promoting stem cell adhesion, proliferation, and differentiation [6]. By incorporating dB-ECM into synthetic PCL nanofibrous scaffolds, it was hypothesized that PCL and dB-ECM-blended scaffolds would not only overcome the poor hydrophilicity of PCL, but also introduce bioactive factors, making it more conducive to cell adhesion and subsequent biological processes essential for bone regeneration.

In this study, PCL/dB-ECM nanofibrous scaffolds with different PCL/dB-ECM ratios were fabricated by electrospinning. The microstructure, hydrophilicity, porosity, and mechanical properties of the produced scaffolds were then characterized. In addition, we studied the PCL/dB-ECM nanofibrous scaffolds on proliferation and osteogenic differentiation of rabbit bone mesenchymal stem cells (rBMSCs) as well. Finally, the ability of the scaffolds to promote bone regeneration *in vivo* was investigated via implantation into a rabbit femoral condylar defect model. This study provides new insights into the construction of BTE scaffolds.

Materials and Methods

Decellularization of Cancellous Bone

Cancellous bone was used in the dB-ECM material due to its biocompatibility, highly porous structure, osteoconductivity, compatibility with other materials, and favorable mechanical properties. The decellularization procedure has been described previously [26–28]. Fresh cancellous bone samples were harvested from the femoral heads of five white swine weighing 50–60 kg and aged 6 months, obtained from a local slaughterhouse within 24 h of slaughter. Thereafter, the cancellous bone samples were washed in phosphate-buffer saline (PBS; KGL2206-500, KeyGEN, Nanjing, China) with continuous shaking for 4 h to remove excess blood, and the PBS was replenished every hour. Subsequently, a combination of physical, chemical, and enzymatic treatment was performed to obtain the dB-ECM. Briefly, the cancellous bone samples were frozen at –80 °C until crystal formation followed by thawing at 37 °C for 2 h. This process was repeated two times. Then the samples were soaked in distilled water containing 0.1 % sodium dodecyl sulfate (SDS; 71725, Sigma-Aldrich, St. Louis, MO, USA) at 37 °C for 24 h. Afterwards, the samples were washed for 30 min in PBS to completely remove SDS, with solution being replenished every 10 min. After being incubated in 1 % Triton X-100 (T8787, Sigma-Aldrich, St. Louis, MO, USA) for 48 h, the samples were degreased with methyl alcohol for 24 h. Following a further 30 min wash in PBS, the samples were processed with 100 U/mL DNaseI (10104159001, Sigma-Aldrich, St. Louis, MO, USA) and 50 U/mL RNase (11119915001, Sigma-Aldrich, St. Louis, MO, USA) at 37 °C for 4 h. Finally, after being washed with PBS under continuous shaking for 30 min twice, the dB-ECM was successfully prepared. The samples were dried and stored at 4 °C for further use.

Decellularization Efficiency of dB-ECM

The absence of visible nuclei in tissue sections stained with hematoxylin and eosin (H&E) and 4′,6-diamidino-phenylindole (DAPI) has been suggested as a criterion for successful decellularization [26]. In addition, the amount of residual DNA should be less than 50 ng/mg dry weight of the dECM [29]. Histological and DNA content analyses of the dB-ECM were performed to evaluate the decellularization effect accordingly.

H&E and DAPI Staining

The native bone tissue and dB-ECM were fixed in 4 % paraformaldehyde for 48 h at room temperature, and then decalcified with 10 % ethylenediaminetetraacetic acid (EDTA; 798681, Sigma-Aldrich, St. Louis, MO, USA) at 4 °C, with replenishing the EDTA solution every two days until the samples were soft enough to be sectioned with a scalpel. Then the samples were dehydrated stepwise using ethanol, embedded in paraffin, and sectioned into 5 μm. After deparaffinization, rehydration, and washing in distilled

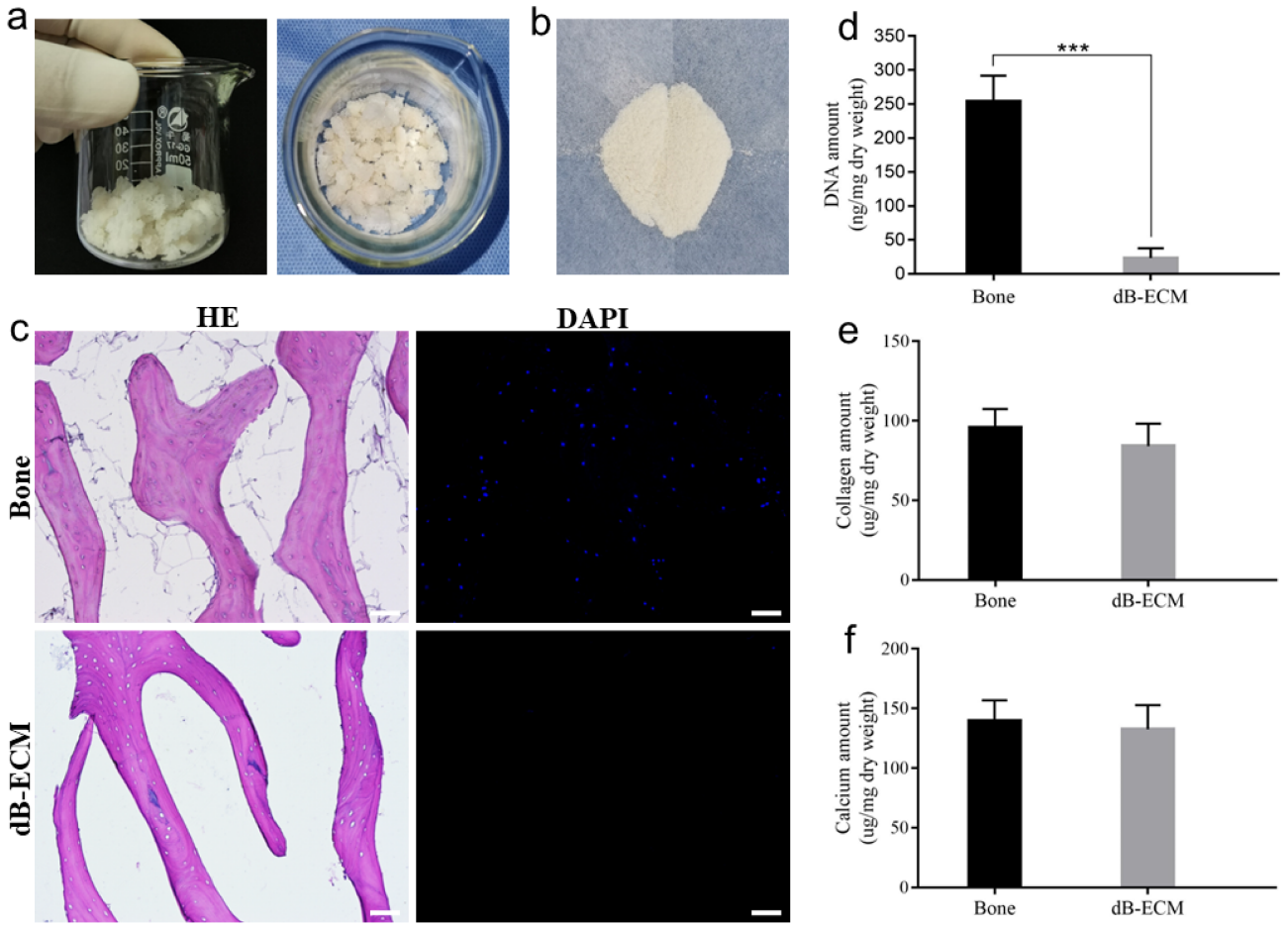

Fig. 1. Preparation and characterization of dB-ECM. (**a**) Gross observation of the dB-ECM. (**b**) dB-ECM powders used in this study. (**c,d**) Evaluation of decellularization effect of dB-ECM by H&E, DAPI staining and DNA quantification. Scale bar = 100 μm, ***$p < 0.001$. (**e,f**) Quantitative analysis of the collagen and calcium in native bone and dB-ECM. Data are presented as the mean ± standard deviation. n = 3 for each group. dB-ECM, decellularized bone extracellular matrix; DAPI, 4′,6-diamino-phenylindole; H&E, hematoxylin and eosin.

water, the slides were stained with H&E to assess the cellular components and general structure of dB-ECM. DAPI staining (KGA1807-100, KeyGEN, Nanjing, China) was performed according to the manufacturer's instructions to detect the presence of residual intact cell nuclei.

Quantification of Residual DNA Amount

To investigate the amount of residual DNA in native bone tissue (n = 6) and dB-ECM (n = 6), a DNA isolation reagent (4461288, Gibco BRL, Gaithersburg, MD, USA) was used to extract genomic DNA according to the manufacturer's instructions. Briefly, equal weights of dried samples were cut into thin strips, and less than 25 mg of tissue was homogenized in 1 mL of DNAzol Reagent, followed by DNA precipitation, DNA washing, and solubilization. The extracted genomic DNA was quantified by measuring the absorbance at 260 nm using a multifunctional microplate reader (Synergy lx, BioTek, Winooski, VT, USA). The DNA content was calculated according to the DNA concentration and initial dry weight of the samples and was presented as ng/mg.

Collagen and Calcium Content Analysis

To evaluate the retention of bioactive components in dB-ECM, collagen and calcium contents were also determined.

A Hydroxyproline assay kit (ml077290, KeyGEN, Nanjing, China) was used to quantify the collagen content of the native bone tissue and dB-ECM according to the manufacturer's instructions and previous studies [30,31]. The native bone tissue (n = 6) and dB-ECM (n = 6) were weighed to achieve equal weights. Then the samples were acid hydrolyzed using 6 M hydrochloric acid (HCL) at 100 °C for 8 h followed by neutralization with sodium hydroxide (NaOH). The Edwards and O'Brien method was used to quantify the hydroxyproline content. Briefly, standard concentrations were prepared using trans-4-hydroxy-L-proline. Then 100 μL Oxidation solution (Chloramine-T in distilled

Table 1. Primer sequences used for qRT-PCR.

Genes	Forward (5′–3′)	Reverse (5′–3′)
GAPDH	TCACCATCTTCCAGGAGCGA	CACAATGCCGAAGTGGTCGT
Col1	CTTCTGGCCCTGCTGAAAGGATG	CCCGGATACAGGTTTCGCCAGTAG
Runx2	TCAGGCATGTCCCTCGGTAT	TGGCAGGTAGGTATGGTAGTGG
Ocn	CCGGGAGCAGTGTGAGCTTA	TCAGGCATGTCCCTCGGTAT
Opn	CACCATGAGAATCGCCGT	CGTGACTTTGGGTTTCTACGC
Bsp	CCTCTTCACTCCAGGACAGC	CACTGCTCGGAACTGGAAACC

Col1, collagen type 1; *Runx2*, runt-related transcription factor 2; qRT-PCR, quantitative real-time reverse transcription polymerase chain reaction.

water) was added to each standard and test sample (50 μL) in a flat bottom 96-well plate with agitation for 5 min. Ehrlich's reagent (100 μL) was then added and the plate was incubated at 60 °C for 45 min. The absorbance was read at 570 nm using a multifunctional microplate reader (Synergy lx, BioTek, Winooski, VT, USA). The hydroxyproline concentration in the samples was determined using an established standard curve. A collagen-to-hydroxyproline ratio of 7.2:1 was used to calculate collagen content in the samples.

The native bone and dB-ECM samples were ground into tiny particles using a mortar and pestle. An equal weight of lyophilized native bone and dB-ECM particles were solubilized in 0.5 M HCL at 4 °C until no visible particles remained. The calcium content of the solution was quantified by inductively coupled plasma optical emission spectrometer (ICP-OES; Thermo Fisher Scientific, Waltham, MA, USA).

Fabrication of Nanofibrous Scaffolds

Nanofibrous scaffolds were fabricated by electrospinning. Three groups of nanofibrous scaffolds were used in this study: PCL, PCL/dB-ECM (4:1), and PCL/dB-ECM (2:1). For the PCL nanofibrous scaffold, a 12 % (w/v) PCL solution was prepared by dissolving PCL particles (molecular weight 80,000; 900288, Sigma-Aldrich, St. Louis, MO, USA) in 1,1,1,3,3,3-hexafluoro-2-propanol (HFP; H107501, Aladdin, Shanghai, China) for 12 h at room temperature with continuous agitation. The PCL solution was then transferred to a 5 mL syringe with 16 gauge blunt-ended needle and positioned in a syringe pump at a flow rate of 1.0 mL/h for the electrospinning process. Aluminum foil was placed at 15 cm distance from the spinneret as a collector. A voltage of 20 KV was applied between the needle and ground collector. For the PCL/dB-ECM (4:1) and PCL/dB-ECM (2:1) nanofibrous scaffolds, dB-ECM particles were ground using a mortar and filtered through a 150-mesh screen to obtain dB-ECM powders. The dB-ECM powders were then added to a 12 % (w/v) PCL solution to obtain blend solutions with different weight ratios of PCL to dB-ECM (4:1 and 2:1, respectively). Following constant stirring, a uniform suspension without aggregation was obtained and injected into a syringe. The same procedure was used to fabricate PCL/dB-ECM (4:1) and PCL/dB-ECM (2:1) nanofibrous scaffolds using electrospinning. Electrospinning was performed at room temperature and 40 % humidity. The scaffolds were removed from the collector, dried overnight in a vacuum oven, and stored in a desiccator until further use.

Characterization of Nanofibrous Scaffolds

Microstructure of Nanofibrous Scaffolds

The nanofibrous scaffolds were cut into 5 × 5 mm discs and gold-coated using a gold sputter coater. The morphology of the nanofibrous scaffolds was observed by scanning electron microscope (SEM; FEI Sirion-100, FEI, Hillsboro, OR, USA) at a voltage of 15 KV. The distribution of calcium (Ca) and phosphorus (P) in the PCL/dB-ECM (4:1) and PCL/dB-ECM (2:1) nanofibrous scaffolds was detected using an energy-dispersive spectrometer (EDS; Oxford Azter X-Max 80) coupled with SEM. The diameter distribution range and average diameter of the nanofibers were calculated by randomly measuring 50 fibers from the SEM micrographs using ImageJ software (Version 1.52, National Institutes of Health, Bethesda, MD, USA).

Water Contact Angle Measurement

The water contact angle (WAR) analysis system (SL200B; Solon Technology Science, Shanghai, China) was used to evaluate the hydrophilic property of the nanofibrous scaffolds. In brief, 0.8 μL of distilled water was dropped onto the surface of scaffolds (15 mm × 15 mm), and the angles between the water droplet and scaffold surface were measured. Six samples from each group were tested. The procedure was performed at room temperature and 50 % humidity.

Porosity Measurement

AutoPore IV-9500 Mercury Porosimeters (AutoPore IV 9500, Micromeritics, Norcross, GA, USA) and mercury porosimetry analysis techniques were used to evaluate the porosity of the nanofibrous scaffolds according to the manufacturer's instructions. All measurements were obtained from six different samples from each group.

Mechanical Characterization

The tensile strength of the nanofibrous scaffolds was measured using a universal material tester (Jitai-utm20knm, Jimtec, Beijing, China). Briefly, samples from different groups were cut into rectangular shapes with dimensions of 20 mm × 30 mm and then clamped to the device with two tensile grips. The tensile strength was measured under a 10 N tensile load and a tensile speed of 1 mm/min. The stress-strain curves of the samples were recorded. According to the stress-strain curves, the ultimate tensile strength was obtained as the highest stress prior to the sample breaking. The elastic modulus was determined as the slope of the initial linear section of the curve, and the elongation (%) was calculated as the percentage elongation of the samples at break.

In Vitro Experiments

Cell Culture of rBMSCs

Four New Zealand white rabbits, aged 3 months, were selected for extraction of primary BMSCs. rBMSCs were isolated as previously described [32]. rBMSCs were cultured in Dulbecco's modified eagle medium (DMEM; 1210046, Gibco BRL, Gaithersburg, MD, USA) containing 10 % fetal bovine serum, 100 U/mL penicillin and 100 mg/mL streptomycin at 37 °C, 5 % CO_2 and 95 % humidity. The culture medium was replenished every 3 days. All biological and technical experiments were conducted in triplicates.

Cell Seeding

Three groups of nanofibrous scaffolds were punched to obtain disks with diameters of 6 mm, which were then placed in 96-well plates. The scaffolds were sterilized by exposing each side to UV light for 1 h, followed by immersion in 75 % ethanol for 2 h, and washing with PBS three times before cell seeding. rBMSCs were seeded on top of the scaffolds at a density of 31,250 cells/cm^2. To facilitate initial cell attachment, the cell-seeded scaffolds were incubated for 6 h. Subsequently, the scaffolds from each group were transferred to fresh culture plates and fresh culture medium was added to continue the cultivation. The medium was replenished every three days.

Cell Proliferation

The cell proliferation of rBMSCs seeded on scaffolds at 1, 3, 5, and 7 days was evaluated using a cell counting kit-8 (CCK-8; PA137267, Thermo Fisher Scientific, Waltham, MA, USA) according to the manufacturer's instructions. Briefly, 20 μL CCK-8 agent was added into each well and cultured with rBMSCs seeded scaffolds at 37 °C, 5 % CO_2 and 95 % humidity for 4 h. After incubation, 200 μL solution of each well was transferred to a new 96-well plate. The absorbance was measured at 450 nm excitation wavelength using a multifunctional microplate reader (Synergy lx, BioTek, Winooski, VT, USA). rBMSCs cultured in 96-well plates without the nanofibrous scaffolds were used as positive controls.

Cell Viability

The cytotoxicity of the scaffolds was evaluated using the Live-Dead kit (L7010, Thermo Fisher Scientific, Waltham, MA, USA) 3 and 7 days after rBMSCs were seeded on the scaffolds according to the manufacturer's instructions. Briefly, at the designed time points, the scaffolds were washed with PBS three times and incubated with a staining solution of 4 mM calcein acetoxymethyl ester and 2 mM ethidium homodimer for 30 min at 37 °C away from light. After gently rinsing three times with PBS, the scaffolds were observed, and images were captured using a confocal laser scanning microscope (CLSM; LSM700, Carl Zeiss, Karlsruhe, Baden-Württemberg, Germany). The viability of representative surface cells from each group was quantitatively analyzed using ImageJ software (National Institutes of Health, Bethesda, MD, USA). During the analysis, the regions of live cells were labeled with one color, and the cells were counted. Similarly, dead cells were marked with another color, and counted. Finally, cell viability was estimated by calculating the ratio of live cells to the total number of cells.

Cell Morphology

After 3 and 7 days of seeding on the scaffolds, the rBMSCs attachment status and morphology were assessed using SEM. Scaffolds were washed with PBS, fixed in 4 % paraformaldehyde for 2 h, and dehydrated using a series of graded ethanol concentrations (70 %, 80 %, 90 %, and 100 %). The samples were dried in air, followed by gold sputter coating. The morphologies of the samples were observed using scanning electron microscope (SEM; FEI Sirion-100, FEI, Hillsboro, OR, USA).

F-Actin Staining

The rBMSCs attachment on the scaffolds and the cytoskeletal morphology were analyzed using F-actin staining. After culturing with rBMSCs for three or seven days, the scaffolds were gently rinsed three times with PBS, and fixed with 4 % paraformaldehyde for 15 min. After being permeabilized with 0.1 % Triton X-100 for 5 min, CoraLite® 594 conjugated phalloidin (PF0003, Proteintech, Rosemont, IL, USA) was used to stain the cytoskeletal protein for 20 min at room temperature. Nuclei were counterstained with DAPI (KGA1807-100, KeyGEN, Nanjing, China) in the dark for 15 min at room temperature. The spread and extension of the rBMSC cytoskeleton were observed, and images were captured using an inverted fluorescence microscope (Axio Observer A1, Carl Zeiss, Karlsruhe, Baden-Württemberg, Germany).

Osteogenic Differentiation of rBMSCs on Nanofibrous Scaffolds

To evaluate the effect of the scaffolds on the osteogenic differentiation of rBMSCs *in vitro*, the following experiments were performed.

Alkaline Phosphatase (ALP) Activity Analysis

Seven days after rBMSCs were seeded on the scaffolds, cells were cultured in an osteogenic induction medium. DMEM high glucose complete medium was used to prepare the osteogenic induction medium, and components such as dexamethasone (10 nM, ST1254, Beyotime, Shanghai, China), vitamin C (50 μg/mL, ST1434, Beyotime, Shanghai, China), and β-glycerophosphate (10 mM, ST637, Beyotime, Shanghai, China) sodium were added to the medium to induce differentiation of stem cells. The azo coupling method was used to evaluate ALP activity using an alkaline phosphatase staining solution (G1480, Solarbio, Beijing, China), according to the manufacturer's instructions. Briefly, the scaffolds were gently rinsed with PBS and fixed with an ALP stationary solution for 3 min. After washing with PBS for 15 s, the scaffolds were incubated in an ALP incubation solution for 15 min, followed by washing with PBS. ALP-positive staining was observed using an optical microscope, and images were captured. Semi-quantitative analysis of ALP activity was performed using a Bicinchoninic Acid assay kit (P0012, Beyotime, Shanghai, China) according to our previous study [32]. The ALP activity level was normalized to the total protein content, and expressed as μmol/hr/mg protein.

Alizarin Red S (ARS) Staining

ARS staining was performed to assess the calcium deposition on the rBMSCs seeded on the scaffolds using an Alizarin Red S Staining Kit (C0148S, Beyotime, Shanghai, China) according to the manufacturer's instructions. PCL/dB-ECM (4:1) and PCL/dB-ECM (2:1) nanofibrous scaffolds without cell culture were also subjected to ARS staining, serving as control 1 group and control 2 group, respectively. Briefly, 21 days after culturing, the scaffolds were rinsed with PBS and fixed with 4 % paraformaldehyde for 20 min. Next, 2 % ARS staining solution was added to the wells for 30 min at room temperature to fully cover the scaffolds. The samples were thoroughly washed with distilled water. Positive staining was observed using an optical microscope and images were captured. Semi-quantitative analysis of the ARS was performed as previously reported [33]. Briefly, 10 % cetylpyridinium chloride (PHR1226, Sigma-Aldrich, St. Louis, MO, USA) was used to decolorize the stain, and the absorbance of the solution was measured at 590 nm using a multifunctional microplate reader (Synergy lx, BioTek, Winooski, VT, USA). ARS levels were normalized to the total protein content.

Quantitative Real-Time Reverse Transcription Polymerase Chain Reaction (qRT-PCR) Analysis of Osteogenic-Related Gene Expression

Osteogenic-related gene expression analysis was performed after the rBMSCs were cultured on the scaffolds for 14 days. Total RNA was extracted from the scaffolds using the TRIzol Reagent (15596026CN, Thermo Fisher Scientific, Waltham, MA, USA). The cells were thoroughly mixed to ensure complete lysis and release of RNA. Chloroform solution was added, then the solution was mixed, and centrifuged. After centrifugation, the aqueous phase (containing RNA) formed the upper layer, whereas precipitated proteins and impurities formed the lower layer. The aqueous phase was then transferred to a new centrifuge tube. Equal volumes of isopropanol were added, then the solution was mixed, and centrifuged to precipitate the RNA. The RNA pellet was washed with 70 % ethanol to remove the residual salts and other impurities. After centrifugation, the ethanol was discarded, and the pellet was air-dried. The RNA pellet was dissolved in diethylpyrocarbonate-treated water. RNA concentration was measured at 260 nm optical density. The RNA was reverse transcribed to cDNA using SuperScript III (18080044, Thermo Fisher Scientific, Waltham, MA, USA). Quantitative PCR was performed with the SYBR Green Reaction Mix (S7585, Thermo Fisher Scientific, Waltham, MA, USA) using a Step One Real-Time PCR System (Thermo Fisher Scientific, Waltham, MA, USA). Triplicates were performed for each sample, and the expressions of target genes were normalized to the corresponding *GAPDH* and analyzed using the $2^{-\Delta\Delta Ct}$ formula. The primer sequences are listed in Table 1.

Immunofluorescence Staining of Osteogenic-Related Proteins

Osteogenesis-related proteins such as collagen type 1 (*Col1*) and runt-related transcription factor 2 (*Runx2*) were detected by immunofluorescence staining to evaluate the osteogenic differentiation of rBMSCs cultured on nanofibrous scaffolds. After 14 days, the scaffolds were fixed in 4 % paraformaldehyde for 1 h, and gently rinsed three times with PBS. After treatment with 0.1 % Triton-X100 (T8787, Sigma-Aldrich, St. Louis, MO, USA) for 15 min, the scaffolds were immersed in 3 % bovine serum albumin (BSA; ST2249, Beyotime, Shanghai, China) for 1 h at room temperature. Then the scaffolds were incubated with primary antibodies (*Col1*, 1:1000; *Runx2*, 1:500; All purchased from Proteintech, Rosemont, IL, USA) at 4 °C overnight followed with incubation of secondary antibodies (CoraLite488-conjugated affinipure goat anti-mouse IgG, 1:500; CoraLite488-conjugated affinipure goat anti-rabbit IgG, 1:500; All purchased from Proteintech, IL, USA) for 1 h at room temperature. To stain the nuclei, DAPI (KGA1807-100, KeyGEN, Nanjing, China) was added onto the scaffolds and incubated for 20 min at room temperature avoiding the light. The scaffolds were then washed three

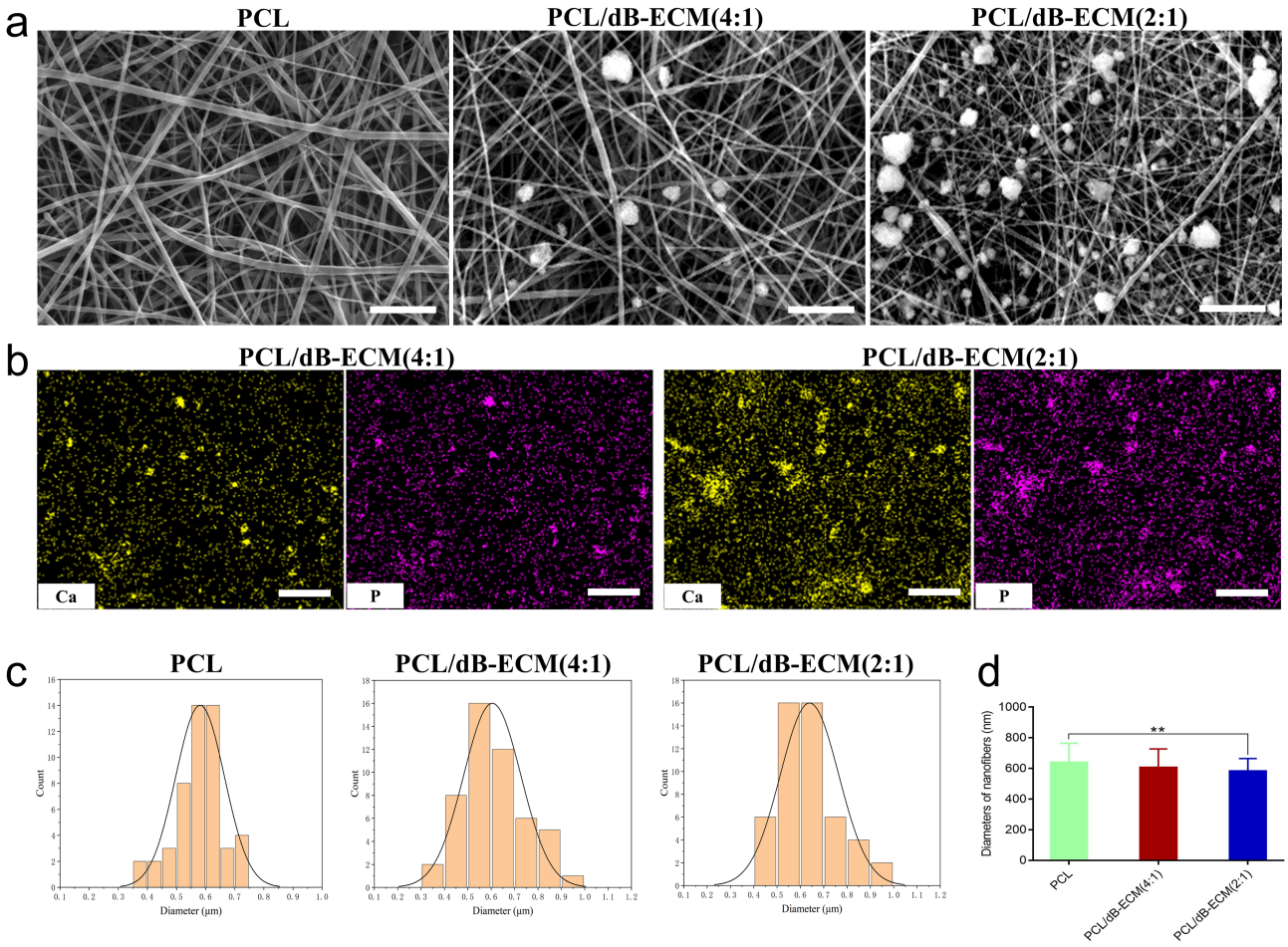

Fig. 2. The microstructure of the nanofibrous scaffolds. (**a**) SEM images of the nanofibrous scaffolds. Scale bar = 10 μm. (**b**) EDS mapping distribution of Ca and P elements in PCL/dB-ECM (4:1) and PCL/dB-ECM (2:1) nanofibrous scaffolds. Scale bar = 25 μm. (**c,d**) The diameter distribution and average diameter of nanofibers in the three groups of scaffolds measured from SEM images with Image J. $^{**}p < 0.01$. Data are presented as the mean ± standard deviation. n = 3 for each group. PCL, poly(ε-caprolactone); Ca, calcium; P, phosphorus; SEM, scanning electron microscope; EDS, energy-dispersive spectrometer.

times, and images were captured using an inverted fluorescence microscope (Carl Zeiss, Baden-Württemberg, Germany). Semi-quantitative analysis of the protein expression of *Col1* and *Runx2* in rBMSCs cultured on nanofibrous scaffolds was performed using ImageJ software (National Institutes of Health, Bethesda, MD, USA) by calculating the mean fluorescence intensity of the images.

In Vivo Animal Model Experiments

A total of 20 female New Zealand white rabbits at the age of six months were used to establish the bone defect model.

The rabbits were randomly divided into scaffold-implanted groups (PCL, n = 5; PCL/dB-ECM (4:1), n = 5; PCL/dB-ECM (2:1), n = 5) and a blank control group (bone defect alone without implants, n = 5). Following general anesthesia by intramuscular injection of 10 % chloral hydrate (4 mL/kg body weight), ketamine (15 mg/kg) was injected intramuscularly after 20–30 min. The knees of the rabbits were shaved and disinfected with iodophor, and a medial parapatellar skin incision was made to expose the femoral condyle. Subsequently, a cylindrical bone defect with a diameter of 4 mm and depth of 4 mm was created using a slow-speed electric drill. To ensure that the defect zone was completely filled, the scaffolds were rolled into a cylinder of the same size as the bone defect and implanted into the defect site. No scaffold was implanted into the blank control group. After washing with sterile normal saline, the knee joint capsule, subcutaneous fascia, and skin were sutured layer by layer with 4-0 absorbable suture.

The rabbits were euthanized at 12 weeks postoperatively, and the femoral condyle was harvested for further analysis.

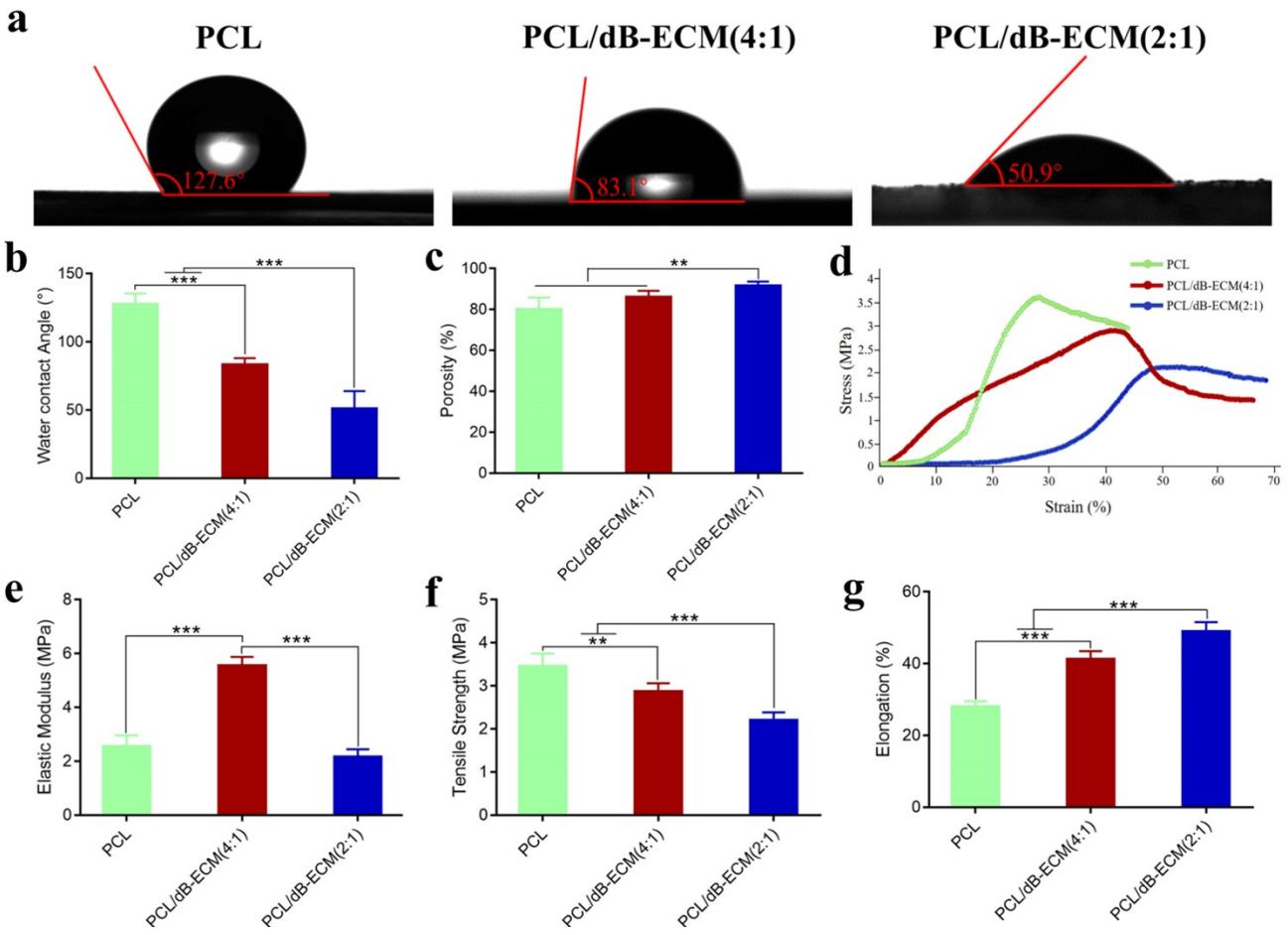

Fig. 3. Hydrophilicity, porosity analysis and mechanical test of the nanofibrous scaffolds. (**a,b**) Water contact angle analysis showing the hydrophilicity of the nanofibrous scaffolds. (**c**) Porosity analysis of the nanofibrous scaffolds. (**d**) Stress-strain curves of the nanofibrous scaffolds. (**e**) Elastic modulus of the nanofibrous scaffolds. (**f**) Tensile strength showing the highest stress prior to the nanofibrous scaffolds break. (**g**) Elongation (%) showing the percentage elongation of the nanofibrous scaffolds at the break. $^{**}p < 0.01$, $^{***}p < 0.001$. Data are presented as the mean ± standard deviation. n = 3 for each group.

Micro-Computed Tomography (Micro-CT) Assessment

Micro-CT was used to assess the formation and density of mineralized tissue at the defect site. The femoral condyle was fixed in 4 % paraformaldehyde for 24 h, and then evaluated by Micro-CT scanner (Inveon Micro, Siemens, Munich, Bavaria, Germany) at a resolution of 15 μm and a voltage of 80 KV. The region of interest (ROI) was defined as a cylinder with a diameter of 4 mm and depth of 4 mm at the bone defect site. The images were analyzed using Micro-CT image analysis software (Version 3.0, Siemens Inveon Research Workplace, Siemens, Munich, Bavaria, Germany), and data, including mineralized callus volume/total callus volume (BV/TV, %), trabecular number (TB.N, 1/mm), trabecular separation (TB.SP, mm), and bone mineral density (BMD) (g/cm^3) were obtained.

Histological Analysis

After the Micro-CT scan was completed, the samples were dehydrated with a graded ethanol series, decalcified in 10 % ethylenediaminetetraacetic acid (EDTA) solution until the blade could easily cut the samples, and embedded in paraffin. The samples were then cut into 5 μm sections for H&E and Masson trichrome staining to evaluate the morphology structure and collagen fibers distribution of the regenerated tissues at the defect site. After staining, the sections were mounted with gum and observed under an optical microscope.

Statistical Analysis

All data are presented as mean ± standard deviation. Student's *t*-test was conducted to evaluate statistical significance between two groups, and one-way Analysis of Variance (ANOVA) was performed for three or more groups. $p < 0.05$ was considered as significant.

Results

Characterization of dB-ECM

Fig. 1 shows the physicochemical properties of the dB-ECM. Gross examination revealed that the dB-ECM appeared as a yellowish-white material (Fig. 1**a**). The dB-

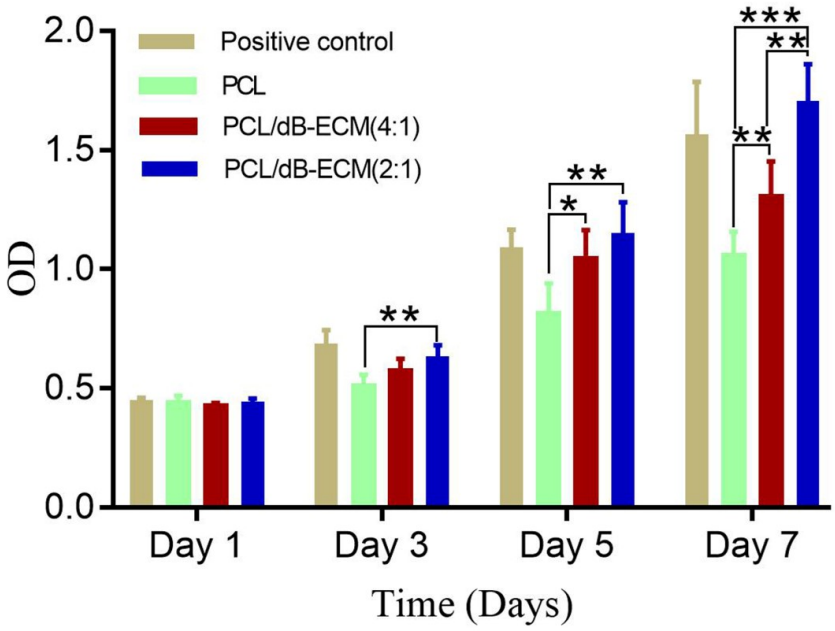

Fig. 4. The CCK-8 results showing the proliferation of rBMSCs cultured on nanofibrous scaffolds at 1, 3, 5 and 7 days, respectively. *$p < 0.05$; **$p < 0.01$; ***$p < 0.001$. Data are presented as the mean ± standard deviation. n = 3 for each group. CCK-8, cell counting kit-8; rBMSCs, rabbit bone mesenchymal stem cells; OD, Optical Density.

ECM was processed into a fine powder by grinding it in a mortar and filtering it through a 150-mesh screen (Fig. 1**b**).

H&E staining, DAPI staining, and DNA quantification were performed to assess the effectiveness of decellularization. H&E staining results (Fig. 1**c**) demonstrated that the nuclei in dB-ECM were nearly completely removed from the cells, whereas the natural architecture and bone matrix remained well-preserved. DAPI staining (Fig. 1**c**) further confirmed the absence of cellular debris. DNA quantification assay showed that native bone tissue contained 253.67 ± 15.58 ng/mg of DNA (Fig. 1**d**), while the dB-ECM retained only 23.17 ± 5.83 ng/mg (Fig. 1**d**). The residual DNA in dB-ECM was below 50 ng, confirming thorough removal of cellular material during decellularization.

The content of collagen and calcium was measured to evaluate the retention of bioactive ingredients in dB-ECM. Collagen content was found to be 95.83 ± 4.97 μg/mg and 84.17 ± 5.74 μg/mg in native bone tissue and dB-ECM, respectively, with no significant difference between the two groups ($p > 0.05$) (Fig. 1**e**). Similarly, no significant difference was found between calcium contents of the native bone tissue and dB-ECM (139.67 ± 6.98 μg/mg and 132.50 ± 8.27 μg/mg, respectively; $p > 0.05$) (Fig. 1**f**).

Overall, these results confirm that the dB-ECM was effectively decellularized while retaining the structural integrity and essential components of the native bone matrix.

Characterization of the Electrospun Nanofibrous Scaffolds

Microstructure of the Nanofibrous Scaffolds

Fig. 2**a** shows the microstructures of PCL-based nanofibrous scaffolds. All scaffolds displayed a network of uniformly thick nanofibers. The PCL/dB-ECM (4:1) and PCL/dB-ECM (2:1) scaffolds showed a relatively even distribution of dB-ECM particles, with minor agglomeration observed. The PCL/dB-ECM (2:1) scaffold contained a noticeably higher quantity of dB-ECM particles than the PCL/dB-ECM (4:1) scaffold, as confirmed by the EDS mapping of calcium (Ca) and phosphorus (P) elements (Fig. 2**b**), which demonstrated a uniform distribution of these elements within the nanofibers. Nanofiber diameters in the PCL/dB-ECM (2:1) scaffold predominantly ranged between 500 and 650 nm, similar to those in the PCL and PCL/dB-ECM (4:1) scaffolds, which ranged from 500 to 700 nm and 400 to 700 nm, respectively (Fig. 2**c**). However, as shown in Fig. 2**d**, the average nanofiber diameter decreased, as the dB-ECM content increased. Specifically, the average diameters were 639.16 ± 124.05 nm for PCL, 604.60 ± 121.54 nm for PCL/dB-ECM (4:1), and 580.90 ± 83.12 nm for PCL/dB-ECM (2:1). There was a significant reduction in the average diameter between the PCL/dB-ECM (2:1) and PCL scaffolds ($p < 0.01$).

Hydrophilicity, Porosity and Mechanical Strength of the Nanofibrous Scaffolds

The PCL scaffold was found to be highly hydrophobic (Fig. 3**a,b**). The water contact angle of the PCL scaffold

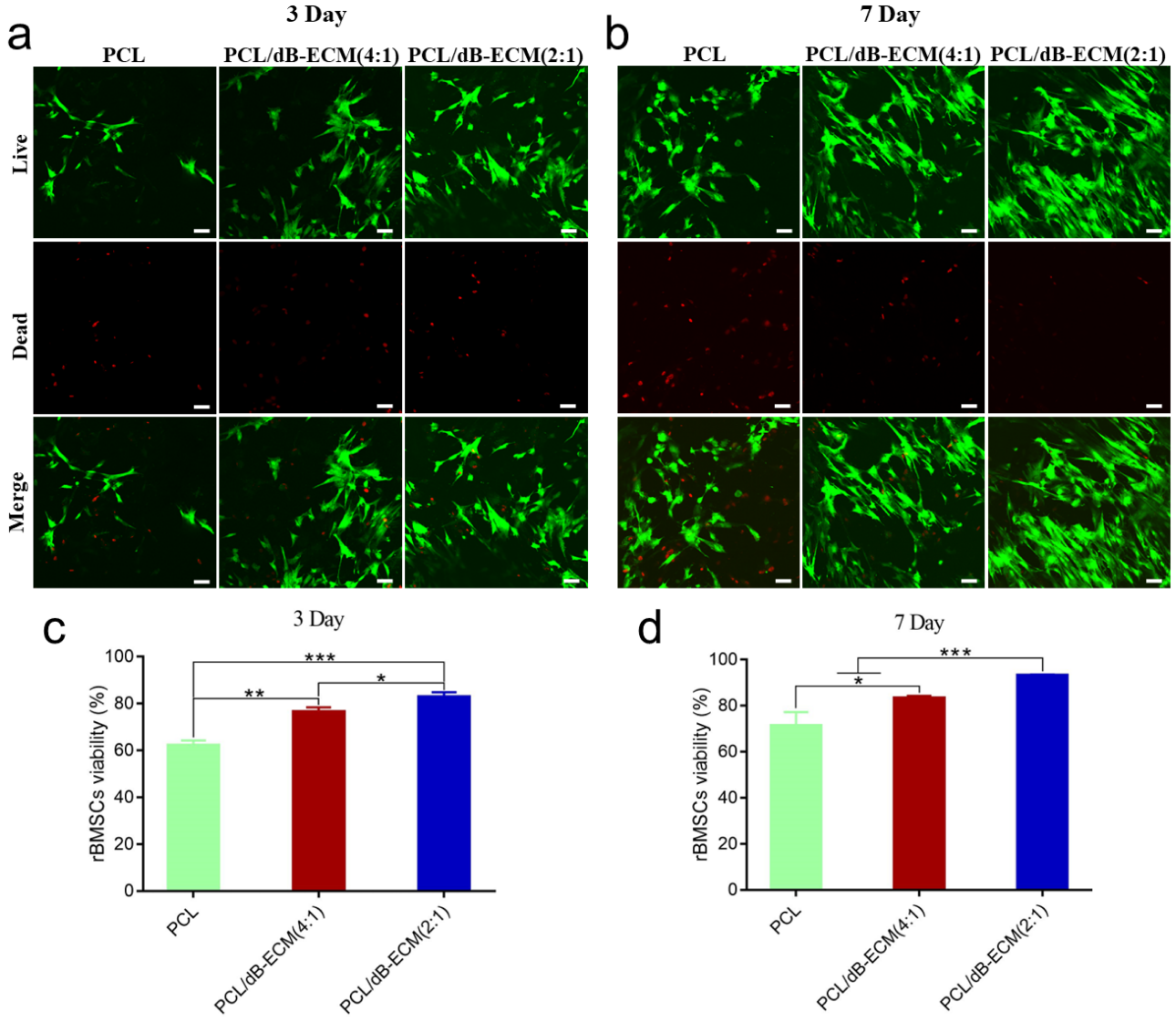

Fig. 5. Cell viability of the nanofibrous scaffolds assessed by Live-Dead staining. (**a**) Representative images of Live-Dead staining showing the viability of rBMSCs cultured on the scaffold surface for 3 days. Scale bar = 50 μm. (**b**) Representative images of Live-Dead staining showing the viability of rBMSCs cultured on the scaffold surface for 7 days. Scale bar = 50 μm. (**c,d**) Quantification of rBMSCs viability calculated from Live-Dead images with Image J after 3 and 7 days cultured on the scaffold surface, respectively. *$p < 0.05$, **$p < 0.01$, ***$p < 0.001$. Data are presented as the mean ± standard deviation. n = 3 for each group.

was found to be 127.61 ° ± 7.48 °. As the dB-ECM content increased, hydrophilicities of the PCL/dB-ECM (4:1) and PCL/dB-ECM (2:1) scaffolds increased, with water contact angles reducing to 83.10 ° ± 4.55 ° and 50.94 ° ± 12.23 °, respectively (Fig. 3**a**). A significant difference was observed between the PCL/dB-ECM (2:1) scaffold and the other two scaffolds ($p < 0.01$) (Fig. 3**b**), indicating that the PCL/dB-ECM (2:1) scaffold had favorable hydrophilic properties.

The porosities (Fig. 3**c**) were found to be 79.99 % ± 5.37 %, 85.93 % ± 2.95 % and 91.42 % ± 2.04 % for PCL, PCL/dB-ECM (4:1) and PCL/dB-ECM (2:1) scaffolds, respectively. Hence, porosity increased as dB-ECM content increased. Compared to the PCL and PCL/dB-ECM (4:1) scaffolds, the PCL/dB-ECM (2:1) scaffold yielded a significantly higher porosity, indicating a higher surface area-to-volume ratio and promotion of cell adhesion.

The mechanical test results are shown in Fig. 3**d–g**. The stress-strain curve (Fig. 3**d**) revealed that the mean elastic modulus of PCL, PCL/dB-ECM (4:1) and PCL/dB-ECM (2:1) scaffolds were 2.53 ± 0.17, 5.54 ± 0.14 and 2.15 ± 0.12 MPa, respectively. The tensile strengths of PCL, PCL/dB-ECM (4:1) and PCL/dB-ECM (2:1) nanofibrous scaffolds were 3.45 ± 0.12, 2.89 ± 0.08 and 2.20 ± 0.08 MPa, respectively (Fig. 3**e,f**). The PCL/dB-ECM (2:1) scaffold thus showed the lowest elastic modulus and tensile strength compared to those of the other scaffolds. In contrast, the elongation rate of PCL/dB-ECM (2:1) scaffold

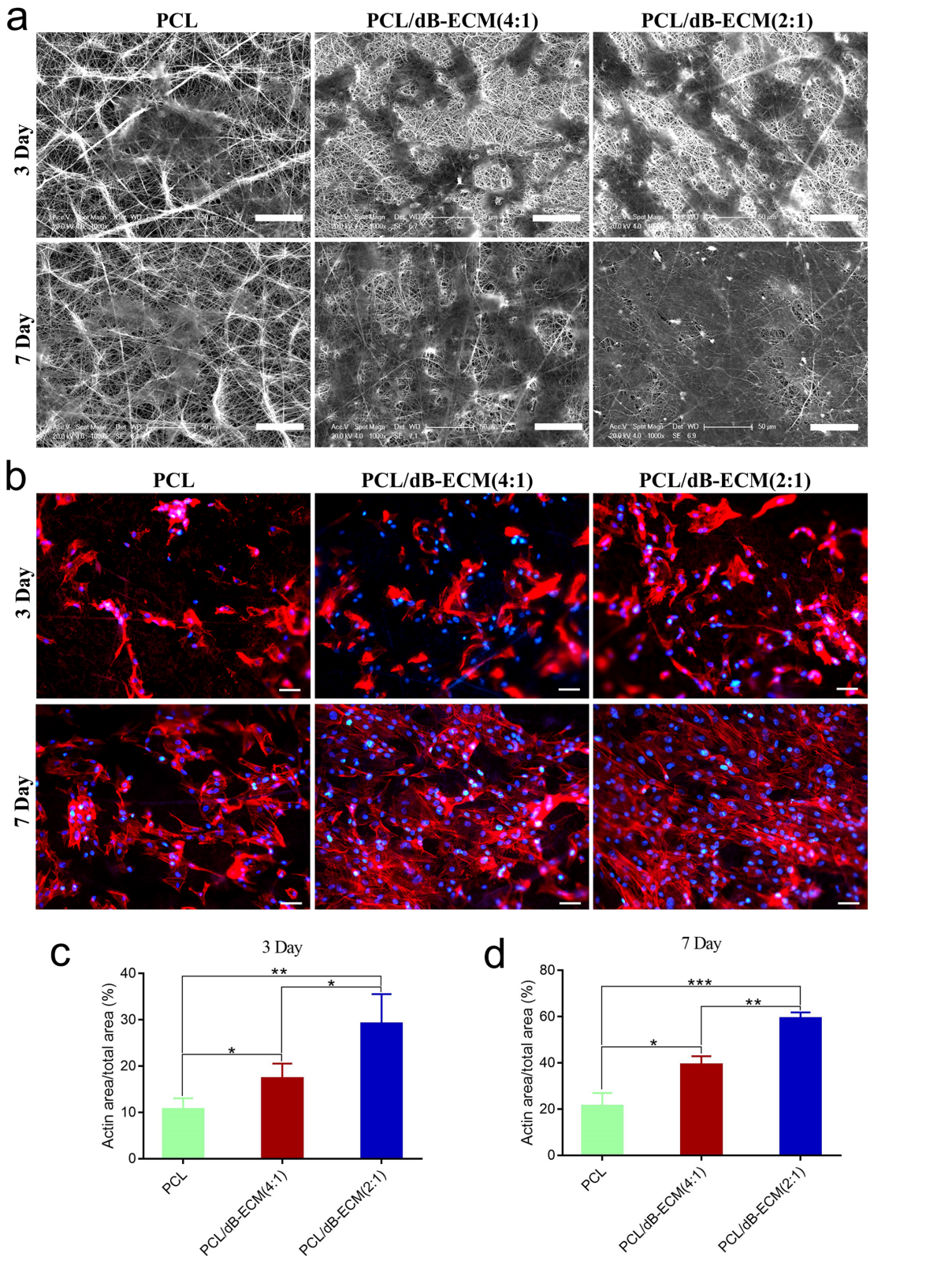

Fig. 6. Evaluation of morphology and cytoskeleton extension of rBMSCs cultured on nanofibrous scaffolds. (**a**) Representative image of SEM showing morphology of rBMSCs cultured on nanofibrous scaffolds for 3 and 7 days. Scale bar = 50 μm. (**b**) Representative images of F-actin staining showing cytoskeleton spread and extension of rBMSCs cultured on nanofibrous scaffolds for 3 and 7 days (red: cytoskeleton, blue: nuclear). Scale bar = 50 μm. (**c,d**) Quantitative analysis of actin area of rBMSCs cultured on nanofibrous scaffolds on day 3 and day 7 calculated from F-actin staining images with Image J. *$p < 0.05$, **$p < 0.01$, ***$p < 0.001$. Data are presented as the mean ± standard deviation. n = 3 for each group.

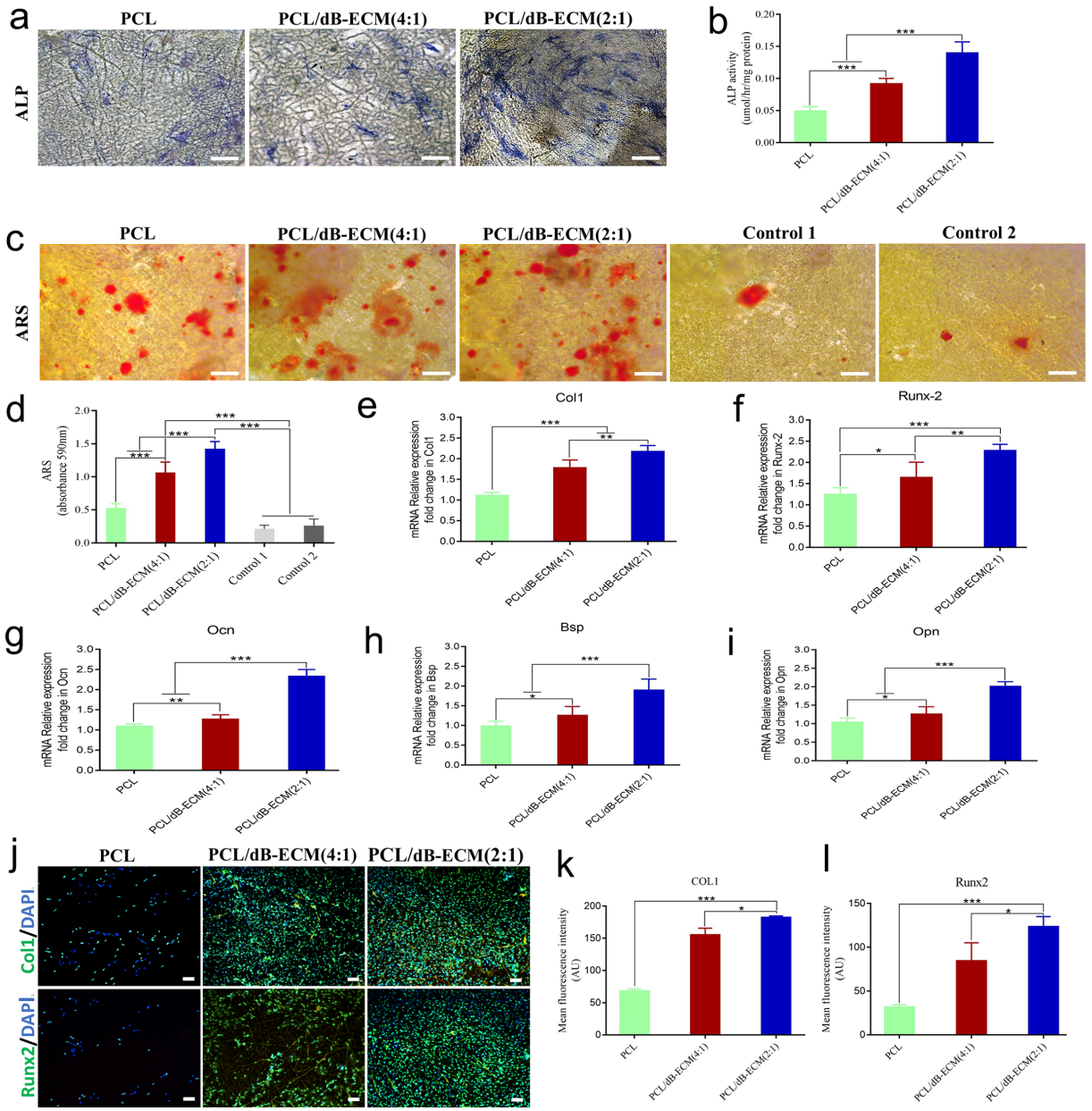

Fig. 7. PCL/dB-ECM (2:1) nanofibrous scaffold promoted osteogenic differentiation of rBMSCs *in vitro*. (**a**) Representative microscopic images showing ALP activity by ALP staining. Scale bar = 100 μm. (**b**) Quantification of ALP activity of rBMSCs cultured on nanofibrous scaffolds on day 7. (**c**) Representative microscopic images showing calcium deposition by ARS staining. Scale bar = 100 μm. (**d**) Quantitative analysis of ARS staining on day 21. (**e–i**) Osteogenic-related genes expression *Col1*, *Runx2*, *Ocn*, *Bsp* and *Opn* analyzed by qRT-PCR. (**j**) Representative immunofluorescent images showing expression of osteogenic-related proteins by rBMSCs cultured on nanofibrous scaffolds for 14 days. Scale bar = 100 μm. (**k,l**) Quantitative analysis of the fluorescence intensity of osteogenic-related proteins *Col1* (k) and *Runx2* (l) analyzed from immunofluorescent images with Image J. *$p < 0.05$, **$p < 0.01$, ***$p < 0.001$. Data are presented as the mean ± standard deviation. n = 3 for each group. ALP, alkaline phosphatase; *Col1*, collagen type 1; *Runx2*, runt-related transcription factor 2; ARS, Alizarin Red S; qRT-PCR, quantitative real-time reverse transcription polymerase chain reaction; AU, Arbitrary Units.

(48.90 % ± 1.10 %) was significantly higher than those of PCL (28.02 % ± 0.61 %) and PCL/dB-ECM (4:1) scaffolds (41.23 % ± 0.91 %) (Fig. 3**g**).

Biological Activities of Nanofibrous Scaffolds In Vitro

Cell Proliferation Results

The proliferation of rBMSCs cultured on the scaffolds was tested at 1, 3, 5, and 7 days after seeding using the CCK-8 assay. Fig. 4 shows that rBMSCs cultured on the scaffolds exhibited increased proliferation rates at all time-

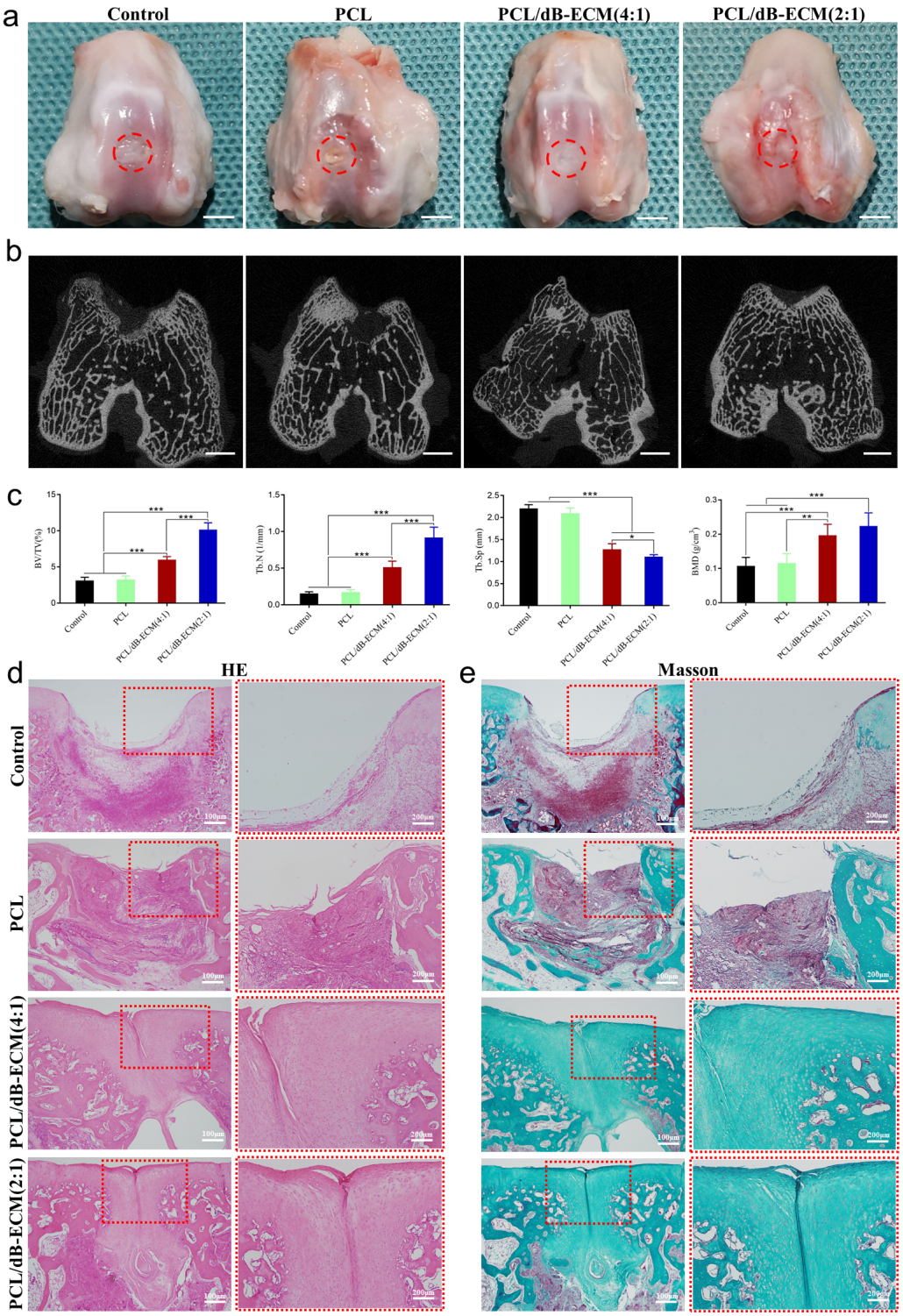

Fig. 8. PCL/dB-ECM (2:1) nanofibrous scaffold promoted osteogenesis *in vivo*. (**a**) Gross observation of rabbit femoral condyle bone defect model repaired with no implant, PCL, PCL/dB-ECM (4:1) and PCL/dB-ECM (2:1) nanofibrous scaffolds. Scale bar = 5 mm. (**b**) Representative Micro-CT images showing the new bone formation and microstructure of the regenerated trabecular within the defect area. Scale bar = 5 mm. (**c**) Quantitative analysis of mineralized callus volume fraction (BV/TV), trabecular number (TB.N), trabecular separation (TB.SP) (BV/TV, %) and bone mineral density (BMD, g/cm^3). (**d**) H&E staining images of regenerated bone tissue at 12 weeks after surgery. (**e**) Masson trichrome staining images of regenerated bone tissue at 12 weeks after surgery. *$p < 0.05$, **$p < 0.01$, ***$p < 0.001$. Data are presented as the mean ± standard deviation. n = 3 for each group. Micro-CT, micro-computed tomography; BV/TV, mineralized callus volume/total callus volume.

points, indicating that the scaffolds had good cytocompatibility. However, the PCL scaffold exhibited the lowest cell proliferation rate throughout the experiment, indicating that the poor hydrophilicity of PCL had a negative effect on cell adhesion and proliferation. Compared with the other two scaffolds, rBMSCs cultured on the PCL/dB-ECM (2:1) scaffolds had the highest cell proliferation rates at both time points, suggesting that the PCL/dB-ECM (2:1) scaffold was the most suitable of the tested scaffolds for rBMSCs proliferation. This may be attributed to the improvement in hydrophilicity of the nanofibrous scaffold upon incorporation of an appropriate amount of dB-ECM, which was previously confirmed by a hydrophilic test of the scaffolds.

Cell Viability Results

A Live-Dead assay was used to evaluate cell viability after culturing the rBMSCs on the nanofibrous scaffolds for 3 and 7 days. Fig. 5**a** shows that after three days, only a small number of dead cells stained with red fluorescence were found in all nanofibrous scaffolds. In contrast, a large amount of green fluorescence stain, which indicates live cells, was observed in the three groups of nanofibrous scaffolds. On day 7, the number of live cells in all the scaffolds increased significantly, further confirming the biocompatibility of the nanofibrous scaffolds (Fig. 5**b**). Notably, rBMSCs cultured on the PCL/dB-ECM (2:1) and PCL/dB-ECM (4:1) nanofibrous scaffolds yielded a significantly higher number of live cells than those cultured on the PCL nanofibrous scaffolds. In particular, the largest number of live cells was found to spread on the surface of the PCL/dB-ECM (2:1) scaffold at both time points compared with the PCL and PCL/dB-ECM (4:1) nanofibrous scaffolds, while the smallest number of dead cells was found, suggesting that the PCL/dB-ECM (2:1) nanofibrous scaffold provided a more suitable microenvironment for promoting rBMSCs proliferation. Fig. 5**c,d** illustrated the quantification of rBMSCs viability calculated from Live-Dead images with Image J after 3 and 7 days cultured on nanofibrous scaffolds, respectively. The viability of rBMSCs reached over 80 % after 3 days of culture on the PCL/dB-ECM (2:1) nanofibrous scaffolds, which was significantly higher than those on the PCL and PCL/dB-ECM (4:1) scaffolds. On day 7, the viability of rBMSCs cultured on PCL/dB-ECM (2:1) scaffold (93.09 ± 0.25 %) also showed significantly higher than that of PCL (71.30 ± 3.40 %) and PCL/dB-ECM (4:1) scaffolds (83.35 ± 0.53 %), indicating that incorporation of appropriate content of dB-ECM enhanced cytocompatibility of the nanofibrous scaffolds.

Cell Morphology Results

The morphology of rBMSCs cultured on nanofibrous scaffolds for 3 and 7 days is shown in Fig. 6**a**. The results revealed that the cells spread flat on all of the nanofibrous scaffolds. Notably, more cells were observed on the surface of the PCL/dB-ECM (2:1) scaffold at both time points compared to the other two scaffolds. After 7 days of culture, the cells on the PCL/dB-ECM (2:1) scaffold stretched and extended to a wider area, covering almost the entire surface of the scaffold. This finding is consistent with our CCK-8 assay (Fig. 4) and Live-Dead results (Fig. 5), and further confirmed that the PCL/dB-ECM (2:1) nanofibrous scaffold had high cytocompatibility and promoted cell attachment and spread.

The cytoskeletal spread and extension of rBMSCs cultured on the nanofibrous scaffolds on days 3 and 7 were evaluated using F-actin staining (Fig. 6**b)**. Compared to the PCL and PCL/dB-ECM (4:1) scaffolds, increased cell attachment onto the PCL/dB-ECM (2:1) scaffolds was observed at both time points, in line with the Live-Dead (Fig. 5) and SEM (Fig. 6**a**) results. Moreover, on day 7, the actin cytoskeleton of rBMSCs cultured on the PCL/dB-ECM (2:1) scaffold showed a wider stretch range and a more parallel arrangement than the PCL and PCL/dB-ECM (4:1) scaffolds. Quantitative analysis of the actin area is illustrated in Fig. 6**c,d**. On day 3, the actin area of rBMSCs cultured on the PCL/dB-ECM (2:1) scaffolds reached nearly 30 %, which is significantly higher than that of the PCL and PCL/dB-ECM (4:1) scaffolds (Fig. 6**c**). On day 7, the actin area of rBMSCs cultured on PCL/dB-ECM (2:1) scaffold (59.23 ± 1.51 %) was also remarkably higher than those of PCL (21.24 ± 3.30 %) and PCL/dB-ECM (4:1) scaffolds (39.18 ± 2.13 %) (Fig. 6**d**). These results further indicated that the incorporation of an appropriate amount of dB-ECM enhanced the adhesion, proliferation, and cytoskeleton extension of rBMSCs on the surface of the scaffolds.

Taken together, these findings indicate that the PCL/dB-ECM (2:1) nanofibrous scaffold is highly cytocompatible for rBMSC growth. Compared to the other two groups of scaffolds, at the early stage of rBMSCs seeding, the incorporation of an appropriate ratio of dB-ECM enhanced cell adhesion, spreading, and cytoskeleton extension on the surface of the PCL/dB-ECM (2:1) scaffold, thereby significantly promoting cell proliferation in the subsequent culture process.

Osteogenic Differentiation of rBMSCs on Nanofibrous Scaffolds

ALP activity was measured to evaluate the osteogenic differentiation of rBMSCs seeded on the nanofibrous scaffolds. Fig. 7**a** shows that the PCL/dB-ECM (2:1) scaffold yielded enhanced osteogenic differentiation than those observed within the PCL and PCL/dB-ECM (4:1) scaffolds. Semi-quantitative analysis of ALP activity (Fig. 7**b)**, revealed a significantly higher ALP activity in the PCL/dB-ECM (2:1) scaffold than in the other two scaffolds.

In addition to the ALP activity assay, ARS staining was also used to assess osteogenic differentiation. Fig. 7**c,d** shows that a remarkably higher calcium deposition in the PCL/dB-ECM (2:1) scaffold was observed compared

to those in the PCL scaffold, PCL/dB-ECM (4:1) scaffold, control 1 and control 2 groups.

To further evaluate the osteogenic differentiation of rBMSCs cultured on different groups of nanofibrous scaffolds, the expression of osteogenic-specific genes in rBMSCs was quantified by qRT-PCR after 14 days of incubation in the osteogenic medium. Fig. 7**e–i** shows that rBMSCs cultured on PCL nanofibrous scaffolds had the lowest expression levels of *Col1*, *Runx2*, *Ocn*, *Bsp*, and *Opn* genes, whereas the expression levels of the same genes were significantly upregulated in rBMSCs cultured on PCL/dB-ECM (4:1) and PCL/dB-ECM (2:1) scaffolds. Notably, the rBMSCs cultured on the PCL/dB-ECM (2:1) scaffold exhibited the highest expression levels of these osteogenesis-specific genes, suggesting that the PCL/dB-ECM (2:1) scaffold significantly enhanced the osteogenic differentiation of rBMSCs.

These results were further confirmed by the immunofluorescence staining of osteogenesis-related proteins (Fig. 7**j**). The PCL/dB-ECM (2:1) scaffold significantly enhanced the protein expression of *Col1* and *Runx2* in rBMSCs compared to the PCL and PCL/dB-ECM (4:1) scaffolds (Fig. 7**j**). As shown in Fig. 7**k,l**, the semi-quantitative analysis, which was expressed as mean fluorescence intensity, displayed notably increased *Col1* and *Runx2* expression in rBMSCs cultured on PCL/dB-ECM (2:1) scaffolds, further indicating that the PCL/dB-ECM (2:1) scaffold significantly promoted the osteogenic differentiation of rBMSCs.

In summary, owing to the incorporation of dB-ECM, rBMSCs cultured on the PCL/dB-ECM (2:1) and PCL/dB-ECM (4:1) scaffolds showed significantly enhanced osteogenic differentiation than those cultured on the PCL scaffold, regardless of the expression level of osteogenic-related genes or proteins. Additionally, the data indicated that the PCL/dB-ECM (2:1) scaffold promoted the osteogenic differentiation of rBMSCs.

In Vivo Implantation

A bone defect model was created in the femoral condyle of rabbits to evaluate the osteogenic effect of the nanofibrous scaffolds *in vivo*. The nanofibrous scaffolds were then implanted in the defect zone, and gross observation, Micro-CT evaluation, and histological assessment were performed 12 weeks post-implantation.

The gross observations showed that the PCL/dB-ECM (2:1) nanofibrous scaffold promoted osteogenesis more strongly compared to the control and other scaffold-implanted groups (Fig. 8**a**). In the control group, the defect zone was covered with the newly formed tissue with an uneven surface, and a circular boundary was clearly visible between the new tissue and native bone tissue. The PCL scaffold was observed to be hardly degraded, and some of the PCL scaffolds remained in the defect area. Even though the defect area was not completely filled with new tissue, the level of healing of the bone defect in the PCL/dB-ECM (4:1) scaffold group was still significantly higher than that in the control and PCL scaffold groups. The bone defect treated with the PCL/dB-ECM (2:1) scaffold showed normal bone morphology, with a healthy-looking and smooth surface. The boundary surrounding the defect zone also disappeared, indicating significant integration between the new tissue and the native bone tissue.

Micro-computed tomography (Micro-CT) analysis was also performed to observe the formation of new bone at the defect site. The control and PCL nanofibrous scaffold groups exhibited insufficient bone regeneration (Fig. 8**b**). In contrast, the PCL/dB-ECM (4:1) and PCL/dB-ECM (2:1) scaffold groups showed significantly higher amount of regenerated bone, with the PCL/dB-ECM (2:1) group showing the most extensive bone regeneration at the defect site (Fig. 8**b**). More importantly, the microscopic aspect of the regenerated trabeculae structure in the PCL/dB-ECM (2:1) scaffold group, such as the arrangement, interconnection, and shape, was more similar to that of the surrounding native trabecular tissues, further indicating significant osteointegration of the PCL/dB-ECM (2:1) scaffold (Fig. 8**b**). The quantitative analysis of new bone formation showed a significantly higher bone volume ratio, trabecular number, and bone mineral density, and lower trabecular separation in the PCL/dB-ECM (2:1) scaffold group than in the control and PCL scaffold groups (Fig. 8**c**). Although new bone formation was notably increased in the PCL/dB-ECM (4:1) scaffold group compared to that in the control and PCL scaffold groups, the bone volume ratio, trabecular number, and bone mineral density were still much lower than those in the PCL/dB-ECM (2:1) scaffold group (Fig. 8**c**).

The Micro-CT results were further corroborated by histological evaluation of new bone formation (Fig. 8**d,e**). Fig. 8**d** shows that the defect site was filled with amorphous and irregular fibrous tissue in the control and PCL scaffold groups, whereas the PCL/dB-ECM (4:1) and PCL/dB-ECM (2:1) scaffold groups showed significantly better trabecular structures, which was consistent with the Micro-CT results (Fig. 8**b**). As shown in the Masson's trichrome staining images in Fig. 8**e**, the PCL scaffold group exhibited several bone collagen fibers that were stained with green at the bottom of the defect site, which was slightly better than that of the control group. However, compared to the PCL/dB-ECM (4:1) and PCL/dB-ECM (2:1) scaffold groups, the PCL scaffold group demonstrated insufficient bone regeneration efficiency. The incorporation of the dB-ECM into the scaffold led to superior regenerated bone with a smooth surface, good trabecular structure, and good integration with the surrounding tissues (Fig. 8**e**). Furthermore, owing to the increase in the dB-ECM content, the PCL/dB-ECM (2:1) scaffold group exhibited significantly higher level of regenerated bone tissue compared to the PCL/dB-ECM (4:1) scaffold group (Fig. 8**e**).

Discussion

Approximately 28 million orthopedic surgery procedures are estimated to be implemented worldwide by 2022. A critical issue in this regard is the increasing demand for bone substitutes, which is the second most transplanted tissue annually [34]. Due to the drawbacks of potential immune response, donor site morbidity, and shortage of supply, autografts and allografts do not fully meet the needs of bone transplantation [35,36]. To this end, BTE, aims to fabricate bioactive bone scaffolds as a substitute for bone tissue, and thus is a promising alternative for repairing bone defects.

Scaffolds, cells, and growth factors are the three main elements of bone tissue engineering strategies. Among these, scaffolds are essential bone regeneration, as they provide a microenvironment suitable for cell adhesion, proliferation, migration, and differentiation [37]. The shape, pore structure, mechanical properties, and biocompatibility of scaffolds directly affect the fate of cells, and subsequently determine the effect of bone regeneration [38,39]. Scaffolds with nanoscale topography are considered promising substrates for bone regeneration, as they imitate the structure of the natural bone extracellular matrix and interlaced collagen fibers, making them more beneficial for cell recruitment and adhesion [40,41]. In this study, nanofibrous scaffolds were fabricated using electrospinning. The results showed that the scaffolds exhibited randomly arranged nanofibers interlaced to form a network structure, which effectively promoted cell diffusion and adhesion, extracellular matrix secretion, and protein adsorption due to a larger specific surface area [42].

The hydrophobic nature of PCL inhibits cell attachment and proliferation [15], which can be resolved by combining it with other biomaterials, such as bioceramics, natural polymers, and inorganic compounds [42,43]. Therefore, different concentrations of dB-ECM were used to prepare PCL/dB-ECM blends, and thus to improve the hydrophilic properties and bioactivity of pure PCL. The findings showed that the PCL nanofibrous scaffold was hydrophobic, and the incorporation of dB-ECM significantly decreased the water contact angle of the PCL/dB-ECM nanofibrous scaffolds. Notably, the water contact angle decreased gradually with an increase in the dB-ECM content, and the PCL/dB-ECM (2:1) scaffold exhibited better hydrophilicity in comparison with the PCL/dB-ECM (4:1) scaffold, highlighting the importance of dB-ECM content in enhancing the hydrophilicity of the PCL/dB-ECM scaffolds. The incorporation of dB-ECM resulted in higher porosity of the PCL/dB-ECM (2:1) scaffold, which enhanced cell proliferation and migration. However, as previously demonstrated, excessive porosity also has certain disadvantages, such as affecting the mechanical properties of the scaffold [42]. The mechanical test results of the present study showed that the PCL/dB-ECM (2:1) scaffold had the lowest elastic modulus and tensile strength, which may be attributed to the incorporation of dB-ECM particles impairing the integrity of the scaffold microstructure. Previous materials used for the same purpose have shown good osteogenic differentiation potential *in vitro*, but failed when implanted *in vivo* due to the imbalance between microstructure and mechanical properties [44]. Therefore, for BTE scaffold fabrication, the mechanical properties need to be considered [44].

Biocompatibility is a key parameter when evaluating the performance of the BTE scaffolds. Lack of biocompatibility may lead to inflammation, immune responses, and tumor formation. The inflammation reaction caused by the scaffold should be resolved within 14 days, otherwise chronic inflammation may result in an infection [44]. Here, chemical, physical, and enzymatic methods were used to obtain a cell-free bone tissue to ensure biocompatibility and to avoid immunogenicity. Characterization of the dB-ECM revealed that this procedure not only achieved a satisfactory decellularization effect but also retained the microstructure and major components of the natural bone ECM, which laid a foundation for subsequent biological experiments. The CCK-8 assay results showed that rBMSCs cultured on the PCL/dB-ECM (2:1) scaffolds exhibited the highest cell viability and proliferation rates after 5 and 7 days of co-culture, suggesting that this scaffold had high biocompatibility, which was further confirmed by the Live-Dead test. After 7 days of culture with rBMSCs, the number of live cells in the PCL/dB-ECM (2:1) scaffold increased significantly compared to that after 3 days of culturing, and the PCL/dB-ECM (2:1) scaffold exhibited the highest number of live cells in comparison with the other scaffolds, with only a few dead cells. Taken together, the incorporation of dB-ECM into the scaffolds did not show any cytotoxicity, indicating the effectiveness of the decellularization process and the safety of dB-ECM. Biological activity assessment further confirmed that the incorporation of dB-ECM enhanced rBMSCs adhesion and proliferation in the nanofibrous scaffolds.

Each tissue has a specific ECM structure and composition that modulates cell response and promotes cell survival within that tissue [28,45]. The ECM exhibits tissue regeneration capabilities by directing seed stem cells to differentiate into tissue-specific cell lines, even without exogenous growth factors [28]. The dB-ECM is a bone-derived biomaterial that can be used alone or in combination with other materials in BTE applications. Compared to other biomaterials, the main advantage of dB-ECM is that it retains the natural microenvironment, biochemical signals, and physiological cues of bone tissue, which can promote cell growth and viability, and thereby promote bone regeneration [27,46,47]. The incorporation of dB-ECM into other biomaterials to fabricate scaffolds could mimic the native bone tissue microenvironment and introduce additional functional groups that may facilitate the initial adhesion and anchoring of cells, and hence providing

an efficient method to construct BTE scaffolds. Numerous studies have demonstrated that scaffolds incorporated with dB-ECM can significantly enhance the expression of osteogenic gene markers when cultured with rBMSCs and promote bone regeneration *in vivo* [48,49]. Consistent with previous findings, the findings obtained here confirmed that the incorporation of dB-ECM not only improves the bioactivity of PCL but also enhances the osteogenic differentiation of rBMSCs *in vitro*. The rBMSCs cultured on the PCL/dB-ECM (2:1) scaffold exhibited higher ALP activity and calcium deposition, as well as upregulated expression of osteogenesis-related genes and proteins. The actin cytoskeleton of rBMSCs cultured on PCL/dB-ECM (2:1) scaffolds showed a more orderly and parallel arrangement than that of the other scaffolds. Thus, incorporation of dB-ECM may have positive effects on the arrangement of the intracellular cytoskeleton, which may be one of the reasons why dB-ECM can enhance cell adhesion and proliferation, an aspect that requires an additional and more in-depth study.

To evaluate new bone formation, a rabbit femoral condyle bone defect model was created, and nanofibrous scaffolds were implanted in the defect site. Micro-CT and histological results showed that the PCL/dB-ECM (2:1) scaffold induced more bone regeneration than the other scaffolds. Remarkably, the newly formed bone tissue exhibited good trabecular microstructure and integrated well with the surrounding native bone tissue. In contrast, the PCL scaffold exhibited insufficient new bone formation. Gross observation revealed that PCL scaffold hardly degraded after 12 weeks of implantation *in vivo*, indicating a potential inhibition of new bone formation. Although biodegradable, PLC takes a long time to completely degrade [50,51], which is not suitable for the construction of BTE scaffolds. The rate of degradation of biomaterials used in the field of BTE is expected to be similar to the rate of bone regeneration. Insufficient degradation rates lead to residual scaffold at the defect site, thus hindering the new bone formation [52,53]. Considering this, the incorporation of dB-ECM into the nanofibrous scaffolds not only improved the bioactivity of PCL but also accelerated the degradation of scaffolds, making them more inclined to promote new bone formation.

This study also has certain limitations. First, although experimental results showed that the addition of dB-ECM facilitated the degradation of PCL materials, the degradation rate could have been influenced by various factors, including the composition of the materials, environmental temperature, humidity, and the *in vivo* environment. Therefore, the precise control of the degradation rate to meet the needs of different application scenarios is an issue that requires further investigation. Second, the mechanical properties of the PCL/dB-ECM nanofiber materials may have been affected by the material ratio and processing techniques. In applications requiring high-strength supports, these materials may not satisfy these requirements. Thus, improving mechanical properties while maintaining biocompatibility and degradation remains challenging. Finally, the preparation of PCL/dB-ECM nanofiber materials may require complex processes and equipment, increasing production costs. Therefore, simplifying the preparation process and improving the product quality are issues that need to be addressed. In summary, although the PCL/dB-ECM nanofiber materials have certain advantages and application potential, there are still some limitations that need to be overcome. Further research and improvements will advance the application of these materials in biomedicine and other fields.

Conclusions

In this study, dB-ECM was successfully prepared using a decellularization process, and subsequently, PCL/dB-ECM nanofibrous scaffolds were fabricated using electrospinning. The microstructures of the PCL/dB-ECM nanofibrous scaffolds exhibited randomly arranged interlaced nanofibers forming a network structure. The incorporation of the dB-ECM into the scaffolds improved the bioactivity of PCL and significantly enhanced the attachment, proliferation, and osteogenic differentiation of rBMSCs. Furthermore, *in vivo* experiment demonstrated that the PC/dB-ECM (2:1) nanofibrous scaffolds remarkably promoted new bone formation. Hence, this study advances our knowledge regarding the construction of dB-ECM-based nanostructured scaffolds and provides a promising strategy for bone defect treatment.

List of Abbreviations

ALP, alkaline phosphatase; ARS, Alizarin Red S; BMD, bone mineral density; BTE, bone tissue engineering; CCK-8, cell counting kit-8; CLSM, confocal laser scanning microscope; *Col1*, collagen type 1; DAPI, 4′,6-diaminophenylindole; dB-ECM, decellularized bone extracellular matrix; DMEM, Dulbecco's modified eagle medium; ECM, extracellular matrix; EDS, energy-dispersive spectrometer; EDTA, ethylenediaminetetraacetic acid; H&E, hematoxylin and eosin; HFP, 1,1,1,3,3,3-hexafluoro-2-propanol; ICP-OES, inductively coupled plasma optical emission spectrometer; Micro-CT, micro-computed tomography; PBS, phosphate-buffer saline; PCL, poly(ε-caprolactone); PLA, poly(lactic acid); PLGA, poly(lactic-co-glycolic acid); ROI, region of interest; *Runx2*, runt-related transcription factor 2; SDS, sodium dodecyl sulfate; SEM, scanning electron microscope; TB.N, trabecular number; TB.SP, trabecular separation; WAR, water contact angle; 3D, three dimension; rBMSCs, rabbit bone mesenchymal stem cells; HCL, hydrochloric acid; qRT-PCR, quantitative real-time reverse transcription polymerase chain reaction; Ca, calcium; P, phosphorus.

Availability of Data and Materials

The raw data of microscopic images of bone sections are deposited to Zenodo and will be publicly available as of the date of publication. All data reported in this paper will also be shared by the lead contact upon request.

Author Contributions

MZ, QZ and LLL contributed to the design of the work and revised the manuscript critically. QSD, JZ and LLL contributed to methodology and biological evaluation. XZ, HH and JCB analyzed the data. XZ, HJS and FRS contributed to acquisition and interpretation of data for the work. MZ and QZ drafted the work. LLL contributed to conceptualization and funding acquisition. All authors contributed to editorial changes in the manuscript, read and approved the final manuscript. All authors agreed to be accountable for all aspects of the work in ensuring that questions related to the accuracy or integrity of any part of the work were appropriately investigated and resolved.

Ethics Approval and Consent to Participate

The animal experiments involved in this study were approved by the ethics committee and Institutional Animal Experiment Committee of Nanjing Medical University (permission number 20220426006).

Acknowledgments

We would like to thank Editage (www.editage.cn) for English language editing.

Funding

This work was supported by Jiangning district Municipal Science and Technology Bureau Foundation (Grant No. 20212021NJNQKJHMJHXM0133) and Nanjing Medical Science and Technique Development Foundation (Grant No. YKK22218).

Conflict of Interest

The authors declare no competing interests. This article has already been uploaded to a preprint (https://doi.org/10.21203/rs.3.rs-2148105/v1).

References

[1] Rocha T, Cavalcanti AS, Leal AC, Dias RB, da Costa RS, Ribeiro GO, *et al*. PTH_{1-34} improves devitalized allogenic bone graft healing in a murine femoral critical size defect. Injury. 2021; 52: S3–S12. https://doi.org/10.1016/j.injury.2021.03.063.

[2] Schemitsch EH. Size Matters: Defining Critical in Bone Defect Size. Journal of Orthopaedic Trauma. 2017; 31: S20–S22. https://doi.org/10.1097/BOT.0000000000000978.

[3] Baldwin P, Li DJ, Auston DA, Mir HS, Yoon RS, Koval KJ. Autograft, Allograft, and Bone Graft Substitutes: Clinical Evidence and Indications for Use in the Setting of Orthopaedic Trauma Surgery. Journal of Orthopaedic Trauma. 2019; 33: 203–213. https://doi.org/10.1097/BOT.0000000000001420.

[4] Altunbek M, Afghah SF, Fallah A, Acar AA, Koc B. Design and 3D Printing of Personalized Hybrid and Gradient Structures for Critical Size Bone Defects. ACS Applied Bio Materials. 2023; 6: 1873–1885. https://doi.org/10.1021/acsabm.3c00107.

[5] Sohn HS, Oh JK. Review of bone graft and bone substitutes with an emphasis on fracture surgeries. Biomaterials Research. 2019; 23: 9. https://doi.org/10.1186/s40824-019-0157-y.

[6] Rindone AN, Nyberg E, Grayson WL. 3D-Printing Composite Polycaprolactone-Decellularized Bone Matrix Scaffolds for Bone Tissue Engineering Applications. Methods in Molecular Biology. 2018; 1577: 209–226. https://doi.org/10.1007/7651_2017_37.

[7] Alcala-Orozco CR, Mutreja I, Cui X, Hooper GJ, Lim KS, Woodfield TBF. Hybrid biofabrication of 3D osteoconductive constructs comprising Mg-based nanocomposites and cell-laden bioinks for bone repair. Bone. 2022; 154: 116198. https://doi.org/10.1016/j.bone.2021.116198.

[8] Carvalho MS, Silva JC, Udangawa RN, Cabral JMS, Ferreira FC, da Silva CL, *et al*. Co-culture cell-derived extracellular matrix loaded electrospun microfibrous scaffolds for bone tissue engineering. Materials Science & Engineering. C, Materials for Biological Applications. 2019; 99: 479–490. https://doi.org/10.1016/j.msec.2019.01.127.

[9] Tebyanian H, Norahan MH, Eyni H, Movahedin M, Mortazavi SJ, Karami A, *et al*. Effects of collagen/β-tricalcium phosphate bone graft to regenerate bone in critically sized rabbit calvarial defects. Journal of Applied Biomaterials & Functional Materials. 2019; 17: 2280800018820490. https://doi.org/10.1177/2280800018820490.

[10] Smith JA, Mele E. Electrospinning and Additive Manufacturing: Adding Three-Dimensionality to Electrospun Scaffolds for Tissue Engineering. Frontiers in Bioengineering and Biotechnology. 2021; 9: 674738. https://doi.org/10.3389/fbioe.2021.674738.

[11] Vesvoranan O, Anup A, Hixon KR. Current Concepts and Methods in Tissue Interface Scaffold Fabrication. Biomimetics. 2022; 7: 151. https://doi.org/10.3390/biomimetics7040151.

[12] Hong J, Yeo M, Yang GH, Kim G. Cell-Electrospinning and Its Application for Tissue Engineering. International Journal of Molecular Sciences. 2019; 20: 6208. https://doi.org/10.3390/ijms20246208.

[13] Li Y, Tian J, Yang C, Hsiao BS. Nanocomposite Film Containing Fibrous Cellulose Scaffold and Ag/TiO_2 Nanoparticles and Its Antibacterial Activity. Polymers. 2018; 10: 1052. https://doi.org/10.3390/polym10101052.

[14] Patel KD, Kim TH, Mandakhbayar N, Singh RK, Jang JH, Lee JH, *et al*. Coating biopolymer nanofibers with carbon nanotubes accelerates tissue healing and bone regeneration through orchestrated cell- and tissue-regulatory responses. Acta Biomaterialiaialia. 2020; 108: 97–110. https://doi.org/10.1016/j.actbio.2020.03.012.

[15] Bharadwaz A, Jayasuriya AC. Recent trends in the application of widely used natural and synthetic polymer nanocomposites in bone tissue regeneration. Materials Science & Engineering. C, Materials for Biological Applications. 2020; 110: 110698. https://doi.org/10.1016/j.msec.2020.110698.

[16] Filippi M, Born G, Chaaban M, Scherberich A. Natural Polymeric Scaffolds in Bone Regeneration. Frontiers in Bioengineering and Biotechnology. 2020; 8: 474. https://doi.org/10.3389/fbioe.2020.00474.

[17] Aldemir Dikici B, Dikici S, Reilly GC, MacNeil S, Claeyssens F. A Novel Bilayer Polycaprolactone Membrane for Guided Bone Regeneration: Combining Electrospinning and Emulsion Templating. Materials. 2019; 12: 2643. https://doi.org/10.3390/ma12162643.

[18] Liu X, Ma Y, Chen M, Ji J, Zhu Y, Zhu Q, *et al*. Ba/Mg co-doped hydroxyapatite/PLGA composites enhance X-ray imaging and bone defect regeneration. Journal of Materials Chemistry. B. 2021; 9: 6691–6702. https://doi.org/10.1039/d1tb01080h.

[19] Kosowska K, Krzysztoforski J, Henczka M. Foaming of PCL-Based Composites Using $scCO_2$-Biocompatibility and Evaluation for Biomedical Applications. Materials. 2022; 15: 3858. https://doi.org/10.3390/ma15113858.

[20] Trachtenberg JE, Santoro M, Williams C 3rd, Piard CM, Smith BT, Placone JK, *et al*. Effects of Shear Stress Gradients on Ewing Sarcoma Cells Using 3D Printed Scaffolds and Flow Perfusion. ACS Biomaterials Science & Engineering. 2018; 4: 347–356. https://doi.org/10.1021/acsbiomaterials.6b00641.

[21] Miroshnichenko S, Timofeeva V, Permykova E, Ershov S, Kiryukhantsev-Korneev P, Dvořaková E, *et al*. Plasma-Coated Polycaprolactone Nanofibers with Covalently Bonded Platelet-Rich Plasma Enhance Adhesion and Growth of Human Fibroblasts. Nanomaterials. 2019; 9: 637. https://doi.org/10.3390/nano9040637.

[22] Richbourg NR, Peppas NA, Sikavitsas VI. Tuning the biomimetic behavior of scaffolds for regenerative medicine through surface modifications. Journal of Tissue Engineering and Regenerative Medicine. 2019; 13: 1275–1293. https://doi.org/10.1002/term.2859.

[23] Loyo C, Cordoba A, Palza H, Canales D, Melo F, Vivanco JF, *et al*. Effect of Gelatin Coating and GO Incorporation on the Properties and Degradability of Electrospun PCL Scaffolds for Bone Tissue Regeneration. Polymers. 2023; 16: 129. https://doi.org/10.3390/polym16010129.

[24] Wu X, Ni S, Dai T, Li J, Shao F, Liu C, *et al*. Biomineralized tetramethylpyrazine-loaded PCL/gelatin nanofibrous membrane promotes vascularization and bone regeneration of rat cranium defects. Journal of Nanobiotechnology. 2023; 21: 423. https://doi.org/10.1186/s12951-023-02155-z.

[25] Benders KE, van Weeren PR, Badylak SF, Saris DB, Dhert WJ, Malda J. Extracellular matrix scaffolds for cartilage and bone regeneration. Trends in Biotechnology. 2013; 31: 169–176. https://doi.org/10.1016/j.tibtech.2012.12.004.

[26] Chen G, Lv Y. Decellularized Bone Matrix Scaffold for Bone Regeneration. Methods in Molecular Biology. 2018; 1577: 239–254. https://doi.org/10.1007/7651_2017_50.

[27] Kim JY, Ahn G, Kim C, Lee JS, Lee IG, An SH, *et al*. Synergistic Effects of Beta Tri-Calcium Phosphate and Porcine-Derived Decellularized Bone Extracellular Matrix in 3D-Printed Polycaprolactone Scaffold on Bone Regeneration. Macromolecular Bioscience. 2018; 18: e1800025. https://doi.org/10.1002/mabi.201800025.

[28] Kim YS, Majid M, Melchiorri AJ, Mikos AG. Applications of decellularized extracellular matrix in bone and cartilage tissue engineering. Bioengineering & Translational Medicine. 2019; 4: 83–95. https://doi.org/10.1002/btm2.10110.

[29] Crapo PM, Gilbert TW, Badylak SF. An overview of tissue and whole organ decellularization processes. Biomaterials. 2011; 32: 3233–3243. https://doi.org/10.1016/j.biomaterials.2011.01.057.

[30] Chen K, Lin X, Zhang Q, Ni J, Li J, Xiao J, *et al*. Decellularized periosteum as a potential biologic scaffold for bone tissue engineering. Acta Biomaterialia. 2015; 19: 46–55. https://doi.org/10.1016/j.actbio.2015.02.020.

[31] Wu J, Ding Q, Dutta A, Wang Y, Huang YH, Weng H, *et al*. An injectable extracellular matrix derived hydrogel for meniscus repair and regeneration. Acta Biomaterialia. 2015; 16: 49–59. https://doi.org/10.1016/j.actbio.2015.01.027.

[32] Dong Q, Zhang M, Zhou X, Shao Y, Li J, Wang L, *et al*. 3D-printed Mg-incorporated PCL-based scaffolds: A promising approach for bone healing. Materials Science & Engineering. C, Materials for Biological Applications. 2021; 129: 112372. https://doi.org/10.1016/j.msec.2021.112443.

[33] Wang Z, Lin M, Xie Q, Sun H, Huang Y, Zhang D, *et al*. Electrospun silk fibroin/poly(lactide-co-ε-caprolactone) nanofibrous scaffolds for bone regeneration. International Journal of Nanomedicine. 2016; 11: 1483–1500. https://doi.org/10.2147/IJN.S97445.

[34] Yazdanpanah Z, Johnston JD, Cooper DML, Chen X. 3D Bioprinted Scaffolds for Bone Tissue Engineering: State-Of-The-Art and Emerging Technologies. Frontiers in Bioengineering and Biotechnology. 2022; 10: 824156. https://doi.org/10.3389/fbioe.2022.824156.

[35] Fairag R, Li L, Ramirez-GarciaLuna JL, Taylor MS, Gaerke B, Weber MH, *et al*. A Composite Lactide-Mineral 3D-Printed Scaffold for Bone Repair and Regeneration. Frontiers in Cell and Developmental Biology. 2021; 9: 654518. https://doi.org/10.3389/fcell.2021.654518.

[36] Wang Z, Wang Y, Yan J, Zhang K, Lin F, Xiang L, *et al*. Pharmaceutical electrospinning and 3D printing scaffold design for bone regeneration. Advanced Drug Delivery Reviews. 2021; 174: 504–534. https://doi.org/10.1016/j.addr.2021.05.007.

[37] Hao Z, Song Z, Huang J, Huang K, Panetta A, Gu Z, *et al*. The scaffold microenvironment for stem cell based bone tissue engineering. Biomaterials Science. 2017; 5: 1382–1392. https://doi.org/10.1039/c7bm00146k.

[38] Perez RA, Mestres G. Role of pore size and morphology in musculoskeletal tissue regeneration. Materials Science & Engineering. C, Materials for Biological Applications. 2016; 61: 922–939. https://doi.org/10.1016/j.msec.2015.12.087.

[39] Söhling N, Neijhoft J, Nienhaus V, Acker V, Harbig J, Menz F, *et al*. 3D-Printing of Hierarchically Designed and Osteoconductive Bone Tissue Engineering Scaffolds. Materials. 2020; 13: 1836. https://doi.org/10.3390/ma13081836.

[40] Chahal S, Kumar A, Hussian FSJ. Development of biomimetic electrospun polymeric biomaterials for bone tissue engineering. A review. Journal of Biomaterials Science. Polymer Edition. 2019; 30: 1308–1355. https://doi.org/10.1080/09205063.2019.1630699.

[41] Keshvardoostchokami M, Majidi SS, Huo P, Ramachandran R, Chen M, Liu B. Electrospun Nanofibers of Natural and Synthetic Polymers as Artificial Extracellular Matrix for Tissue Engineering. Nanomaterials. 2020; 11: 21. https://doi.org/10.3390/nano11010021.

[42] Yuan B, Wang Z, Zhao Y, Tang Y, Zhou S, Sun Y, *et al*. *In Vitro* and *In Vivo* Study of a Novel Nanoscale Demineralized Bone Matrix Coated PCL/β-TCP Scaffold for Bone Regeneration. Macromolecular Bioscience. 2021; 21: e2000336. https://doi.org/10.1002/mabi.202000336.

[43] Oh GW, Nguyen VT, Heo SY, Ko SC, Kim CS, Park WS, *et al*. 3D PCL/fish collagen composite scaffolds incorporating osteogenic abalone protein hydrolysates for bone regeneration application: *in vitro* and *in vivo* studies. Journal of Biomaterials Science. Polymer Edition. 2021; 32: 355–371. https://doi.org/10.1080/09205063.2020.1834908.

[44] Perić Kačarević Ž, Rider P, Alkildani S, Retnasingh S, Pejakić M, Schnettler R, *et al*. An introduction to bone tissue engineering. The International Journal of Artificial Organs. 2020; 43: 69–86. https://doi.org/10.1177/0391398819876286.

[45] Frantz C, Stewart KM, Weaver VM. The extracellular matrix at a glance. Journal of Cell Science. 2010; 123: 4195–4200. https://doi.org/10.1242/jcs.023820.

[46] Kabirian F, Mozafari M. Decellularized ECM-derived bioinks: Prospects for the future. Methods: A Companion to Methods in Enzymology. 2020; 171: 108–118. https://doi.org/10.1016/j.ymeth.2019.04.019.

[47] Taylor DA, Sampaio LC, Ferdous Z, Gobin AS, Taite LJ. Decellularized matrices in regenerative medicine. Acta Biomaterialia. 2018; 74: 74–89. https://doi.org/10.1016/j.actbio.2018.04.044.

[48] Golebiowska AA, Intravaia JT, Sathe VM, Kumbar SG, Nukavarapu SP. Decellularized extracellular matrix biomaterials for regenerative therapies: Advances, challenges and clinical prospects. Bioactive Materials. 2024; 32: 98–123. https://doi.org/10.1016/j.bioactmat.2023.09.017.

[49] Smith CA, Board TN, Rooney P, Eagle MJ, Richardson SM, Hoyland JA. Correction: Human decellularized bone scaffolds from aged donors show improved osteoinductive capacity compared to young donor bone. PLoS One. 2017; 12: e0187783. https://doi.org/10.1371/journal.pone.0187783.

[50] Gleadall A, Pan J, Kruft MA, Kellomäki M. Degradation mechanisms of bioresorbable polyesters. Part 1. Effects of random scission, end scission and autocatalysis. Acta Biomaterialia. 2014; 10:

2223–2232. https://doi.org/10.1016/j.actbio.2013.12.039.
[51] Gleadall A, Pan J, Kruft MA, Kellomäki M. Degradation mechanisms of bioresorbable polyesters. Part 2. Effects of initial molecular weight and residual monomer. Acta Biomaterialia. 2014; 10: 2233–2240. https://doi.org/10.1016/j.actbio.2014.01.017.
[52] Malikmammadov E, Tanir TE, Kiziltay A, Hasirci V, Hasirci N. PCL and PCL-based materials in biomedical applications. Journal of Biomaterials Science. Polymer Edition. 2018; 29: 863–893. https://doi.org/10.1080/09205063.2017.1394711.
[53] Yildirimer L, Seifalian AM. Three-dimensional biomaterial degradatio—Material choice, design and extrinsic factor considerations. Biotechnology Advances. 2014; 32: 984–999. https://doi.org/10.1016/j.biotechadv.2014.04.014.

Editor's note: The Scientific Editor responsible for this paper was Matteo D'Este.

Received: 1st February 2024; **Accepted**: 7th November 2024; **Published**: 14th February 2025